Charles University

Faculty of Science

Study programme: Cell Biology

Bc. Viliam Čizmazia

Engineering Linker-Defined Nucleosomal Arrays for Proteomic Profiling

Konstrukce nukleozomů s definovanými linkery pro proteomické profilování

MASTER THESIS

Supervisor: doc. Ing. Václav Veverka, Ph.D.

Prague 2025

I hereby declare that my thesis represents my original research work. Wherever the contribution of others is involved, every effort is made to indicate this clearly, including reference to the literature. This thesis contains no material that has been submitted previously, in whole or in part, for the award of any other academic degree or diploma.

Prague, 1. 8. 2025 Bc. Viliam Čizmazia

Acknowledgements

I would like to express my sincere gratitude to my supervisor Václav Veverka for giving me the opportunity to work on this project, for his trust and guidance throughout its course. I am deeply thankful to Růžena Filandrová and Michal Svoboda for their contributions and guidance, as well as for their advice. My huge thanks also goes to Alexandra Gredová and Vanda Lux for their readiness to help whenever they could. I am grateful to my family for showing trust, interest and support, and to Nina for her love and for brightening up even the most challenging days.

Abstract

Eukaryotic genomes are packaged into chromatin, a dynamic nucleoprotein complex in which nucleosomal units are connected by stretches of linker DNA. Its length is variable, quantized and highly controlled. Spacing strongly influences higher-order chromatin folding, accessibility, DNA integrity and potentially the recruitment of chromatin-associated factors. However, the precise biological reasons why eukaryotes set specific spacing patterns remain largely unknown. To study the impact of internucleosomal spacing on protein interactions in a controlled biochemical setting, a library of DNA constructs was generated based on the Widom 601 nucleosome positioning sequence, with defined linker lengths and compatible cloning sites. The constructs were designed to allow easy multiplication of repeats, enabling the assembly of longer arrays. DNA fragments were biotinylated for immobilization and reconstituted with recombinant histone octamers to yield variably spaced nucleosomes. As a proof of principle, dinucleosomal arrays were immobilized on streptavidin-coated magnetic beads and incubated with nuclear extracts in a pulldown experiment. Captured proteins were analyzed, revealing preliminary insight on protein binding patterns and linker-dependent differences. These experiments establish the feasibility of using this system for quantitative proteomic analysis to map spacing-dependent chromatin interactors. The modular design of the DNA library and labeling strategy makes the system applicable to a range of biochemical and structural methods, biolayer interferometry and cryo-EM. This system provides a versatile tool for dissecting the basis of chromatin-protein interactions with control over the spacing parameter.

Key words

chromatin, linker DNA, spacing, nucleosome reconstitution, proteomics, Widom sequence, nucleosomes

Abstrakt

Eukaryotické genomy jsou uspořádány do chromatinu, dynamického nukleoproteinového komplexu, ve kterém jsou nukleozomové jednotky propojeny úseky spojovací (linker) DNA. Délka těchto úseků je variabilní, kvantovaná a přísně regulovaná. Vzdálenost mezi nukleozomy významně ovlivňuje vyšší úrovně skládání chromatinu, jeho přístupnost, integritu DNA a potenciálně i interakce faktorů asociovaných s chromatinem. Přesné biologické důvody, proč eukaryota nastavují konkrétní vzorce vzdáleností, však zůstávají nepřezkoumané. Pro studium vlivu internukleozomální vzdálenosti na interakce proteinů v kontrolovaném biochemickém prostředí byla vytvořena knihovna DNA konstruktů založená na polohovací sekvenci Widom 601 s definovanou délkou linker DNA a kompatibilními klonovacími místy. Konstrukty byly navrženy tak, aby umožňovaly snadnou propagaci opakujících se jednotek a sestavení delších nukleozomálních řetězců. DNA fragmenty byly značeny biotinem pro imobilizaci a následně rekonstituovány s rekombinantními histonovými oktamery za vzniku nukleozomů s různými délkami linker DNA. Jako ověření funkčnosti byly dinukleozomy imobilizovány na streptavidinových magnetických kuličkách a inkubovány s jadernými extrakty v afinitní purifikaci. Zachycené proteiny byly analyzovány a poskytly předběžný náhled na profily vazby proteinů a rozdíly závislé na délce linker DNA. Tyto experimenty potvrzují použitelnost systému pro kvantitativní proteomickou analýzu s cílem mapovat chromatinové interaktory závislé na tomhle parametru. Modulární konstrukce DNA knihovny a strategie značení činí tento systém využitelným pro široké spektrum biochemických a strukturních metod. Představuje tak univerzální nástroj pro studium základů interakcí chromatinu s proteiny s kontrolou nad parametrem internukleozomální vzdálenosti.

Klíčová slova

chromatin, linker DNA, nukleozomy, rekonstituce nukleozomů, proteomika, Widom sekvence

List of Abbreviations

AE	anion-exchange
bp	base pair
BSA	bovine serum albumin
BW	Binding/Wash Buffer
Chd	chromodomain helicase DNA-binding
CIP	calf intestinal phosphatase
cryo-ET	cryo-electron tomography
CTCF	CCCTC-binding factor
CV	column volume
dATP	deoxyadenosine triphosphate
DCC	DNA Clean & Concentrator
DMEM	Dulbecco's Modified Eagle Medium
DNA	deoxyribonucleic acid
dUTP	deoxyuridine triphosphate
EDTA	ethylenediaminetetraacetic acid
FBA	Fractionation Buffer A
FBS	fetal bovine serum
FPLC	fast protein liquid chromatography
FT	flow-through
GTF	general transcription factor
H1	linker histone H1
H2A	histone H2A
H2A.Bbd	histone H2A Barr body-deficient
H2A.Z	histone H2A variant Z
H2Bub	monoubiquitinated histone H2B
H3	Histone H3
HEK	human embryonic kidney
HF	high-fidelity
I	input
IgG	immunoglobulin G
INO80	ATPase component of the INO80 complex
IR	infrared
ISWI	imitation switch
kb	kilobase
LB	Luria-Bertani medium
LLPS	liquid–liquid phase separation
mAU	milli-absorbance units
MNase	micrococcal nuclease
MOPS	3-(N-morpholino)propanesulfonic acid
Mw	molecular weight
MWCO	molecular weight cut-off
NBB	Nuclear Buffer B
NBC	Nuclear Buffer C
NEB	New England Biolabs
NFR	nucleosome-free region
NRL	nucleosome repeat length

PAGE	polyacrylamide gel electrophoresis
PBS	phosphate-buffered saline
PCR	polymerase chain reaction
PEG	polyethylene glycol
PTM	post-translational modification
pUC19	pUC19 plasmid
PWWP	Pro-Trp-Trp-Pro domain
RB	Reconstitution Buffer
Reb1	RNA polymerase I enhancer binding protein 1
RS1	restriction site 1
RS2	restriction site 2
RS3	restriction site 3
RS4	restriction site 4
rSAP	recombinant shrimp alkaline phosphatase
RSC	remodels the structure of chromatin
SDS	sodium dodecyl sulfate
SEC	size-exclusion chromatography
SN	supernatant
SWI/SNF	Switch/sucrose non-fermentable
TBST	Tris-buffered saline with Tween-20
TSS	transcription start site
UV	Ultraviolet

Contents

1 Introduction

Chromatin is built from repeating nucleosome units connected by stretches of linker DNA. The length of this linker DNA is not random – it is variable but precisely regulated, and displays characteristic patterns across species. Subtle changes in linker length can have profound effects on higher-order chromatin folding, DNA accessibility, genome stability, and the recruitment of chromatin-associated factors. The biological significance of the fine-tuned spacing patterns observed in vivo remains poorly understood. *In vivo*, chromatin-binding proteins interact with nucleosome arrays of varying spacing, but the complexity of the nuclear environment makes it challenging to dissect whether these proteins discriminate between different linker lengths directly. This thesis aims to establish a simplified *in vitro* system for analysis of linker length-specific chromatin interactors.

The eukaryotic genetic material is stored in the nucleus and organized into a complex and dynamic structure of chromatin, with the nucleosome serving as the fundamental repeating unit. A nucleosomal unit consists of around 147 base pairs of DNA wrapped around an octamer of histone proteins (H2A, H2B, H3 and H4, two copies of each), and these units are separated by stretches of linker DNA. Initially, the main purpose of chromatin organization was considered to be compaction and prevention of non-specific aggregation, yet chromatinization of genomic DNA enhances its coding capacity and serves as a crucial regulatory platform for ultimately all DNA-templated processes including replication, transcription, damage repair and more. This tunable platform allows for fast reconstruction to give regulated access to the underlying DNA. It is reliant on nucleosomal composition, associated non-histone factors, the 3D organization and importantly, the post-translational modifications of histones (Misteli, 2007). These take place mainly on the N-terminal unstructured tails of histones, but also on residues of the globular domains (Ng et al., 2002). The chemical modifications among others include acetylation, methylation, phosphorylation, ubiquitination, biotinylation and many more. The enzymes responsible for histone post-translational modifications (PTMs) deposition and removal are often collectively called writers and erasers respectively, and their collective activity creates the so-called histone code, which is then interpreted by reader proteins. Readers are equipped with specialized domains that selectively bind modified histone moieties. The individual chromatin signatures can be complex, and they frequently show combinatorial

readout (Lukauskas et al., 2024), with interplay between the systems responsible for deposition, removal and maintenance of histone PTMs and also with other epigenetic systems like DNA methylation (Jambhekar et al., 2019; Neri et al., 2017). Altogether these signatures define an intricate continuum of functional states with varying degrees of accessibility ranging from closed to open (Klemm et al., 2019). These states provide transcriptional cues with gene bodies and regulatory elements (Nacev et al., 2019). Typically, nucleosomes were known to inhibit transcription as a physical obstacle at promoters. Importantly, they prevent initiation of transcription from cryptic promoter sequences (Kornberg & Lorch, 2020). However, chromatinization of DNA enables more potent and less aberrant transcription than naked DNA. Especially in cooperation with activating histone PTM signatures, such as acetylation and histone H3 lysine 4 trimethylation, nucleosomes can direct the transcriptional machinery to the transcriptional start site (Nagai et al., 2017).

1.1 Nucleosomal Arrays

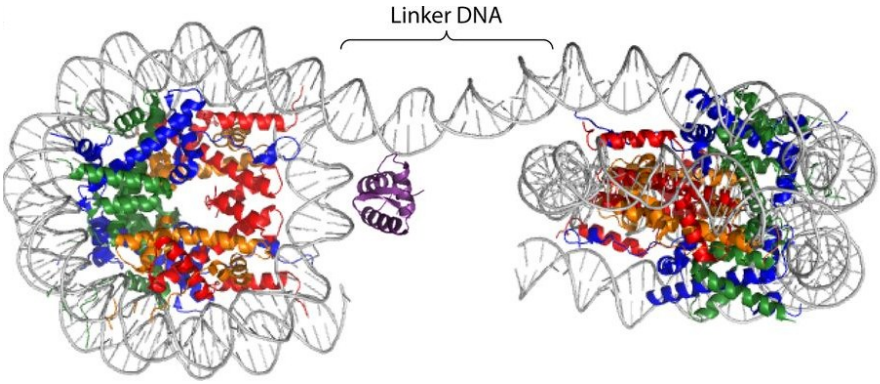

Figure 1. Basic architecture of nucleosomes. Each nucleosome consists of DNA (grey) wrapped around a histone octamer composed of histone H2A (blue), H2B (green), H3 (red), and H4 (orange). The two nucleosomes are connected by a stretch of linker DNA, shown between the two core particles. A linker histone (purple) is bound near the entry/exit site of the DNA on one nucleosome. Adapted from Panday & Grove, (2016).

Nucleosomal units are connected via short variable stretches of linker DNA to form extended arrays. Partial digestion of chromatin by micrococcal nuclease (MNase), which only cleaves in the extranucleosomal regions, produces a typical ladder pattern, which is informative of a variable commonly referred to as the nucleosome repeat length (NRL). It represents the dyad to dyad distance between two nucleosomes, however, it is important to stress that outputs from these mapping experiments only represent average values for the whole genome of a cell population (Baldi et al., 2020). Organization of these arrays is characterized by several interdependent features, including positioning, phasing,

occupancy, and spacing. Positioning refers to the specific placement of nucleosomes along DNA, while phasing describes their alignment relative to genomic landmarks. Nucleosome occupancy measures the frequency of nucleosome presence at specific sites. In contrast, nucleosomal spacing, defined by the NRL or alternatively by linker DNA length, represents the average distance between adjacent nucleosomes.

The primary focus of this thesis is on nucleosomal spacing. Linker lengths vary widely among eukaryotes, with differences observed both across species and among cell types within the same organism, particularly in higher organisms. The shortest known NRL, around 165 bp, has been identified in budding yeast, while the longest, approximately 220 bp, is found in echinoderm sperm. In most vertebrate cells and tissues, the genome-wide NRL typically ranges from 175 to 190 bp, though these values represent average

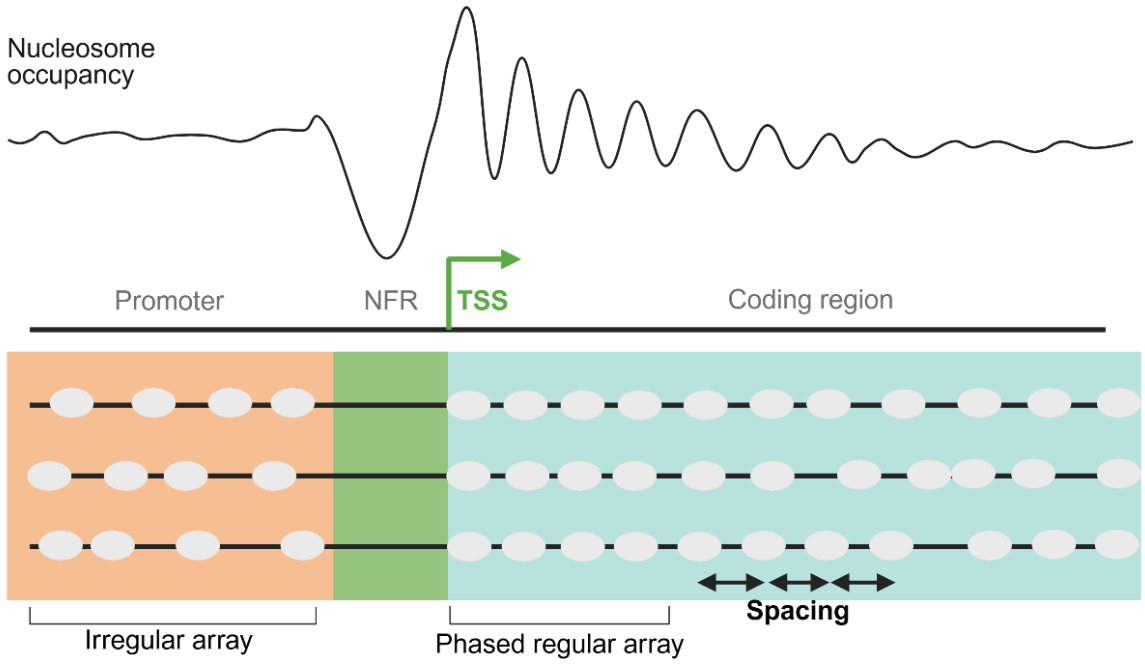

Figure 2. Stereotypical nucleosomal organization around gene units. In yeast and mammals, nucleosome positions around promoters typically display heterogeneously spaced nucleosomes followed by low-occupancy nucleosome-free region just upstream of the transcriptional start site. In mammals the region can be occupied by a fragile nucleosome that is easy to displace during initial remodeling activity. The NFR allows access to general regulatory factors and initiation machinery. Downstream of the NFR is a well-positioned high-occupancy +1 nucleosome and short stretch of regularly spaced nucleosomes. The array regularity gradually decreases further into the gene unit.

lengths and may vary in specific contexts and genomic regions (Brogaard et al., 2012; Clark et al., 2020; Lantermann et al., 2010; Perišić et al., 2010; Valouev et al., 2011). If

linkers within a particular nucleosomal array possess a highly similar length, the array is regarded as regular. Irregular arrays have an undefined NRL. In yeast, nucleosome positioning exhibits distinct linker DNA patterns across gene units (**Figure 2**). Promoter regions typically feature a nucleosome-free region (NFR) upstream of the transcription start site (TSS), facilitating transcription factor access, and a well-positioned +1 nucleosome. Downstream of the NFR, nucleosomes are organized into regularly spaced arrays along the coding regions, with linker DNA lengths contributing to this uniform spacing (Chereji et al., 2018; Lantermann et al., 2010; Yuan et al., 2005). Downstream of +1, nucleosomes form a phased array that gradually decays in regularity over approximately 4 to 6 nucleosomes (spanning ~600-1000 bp) (Mavrich et al., 2008). In mammals, nucleosome organization around gene units displays both similarities and distinctions compared to yeast. Mammalian promoters often exhibit nucleosome-depleted regions (Voong et al., 2016a) or regions containing a “fragile” nucleosome, which is prone to displacement. This low occupancy region, similar to yeast, allows access to regulatory factors. The nucleosomes downstream of +1 are phased, though this regularity gradually diminishes over approximately 5 to 10 nucleosomes, spanning around 1 kb downstream of the TSS (Schones et al., 2008). However, nucleosome spacing in mammals varies more widely (Valouev et al., 2011). In mice cells for example, there are two major trends in nucleosomal organization: nucleosomes in heterochromatin regions, or near silent TSSs, show large variation in positioning (across different cells), but are uniformly spaced along the nucleosome array. Opposingly, nucleosomes near the transcription start sites of active genes show little variation in positioning, but are heterogeneously spaced along the array (Lai et al., 2018). Analysis of nucleosome spacing across different chromatin states in *Drosophila* cells shows clear patterns as well. Regions associated with transcriptional elongation and heterochromatin have the most regularly spaced nucleosomes, while active promoters and enhancers show more disorganized arrays due to nucleosome-free regions and bound transcription factors (Baldi et al., 2018). Importantly, global internucleosomal spacing is biased toward 10n+5 and depleted for 10n bp in yeast and mESC genomes (**Figure 3A**) (Brogaard et al., 2012; Voong et al., 2016).

1.2 Biogenesis of Regular Nucleosomal Arrays

1.2.1 Sequence and Transcription

The precise spacing between nucleosomes in arrays is a function of several mechanisms, though it is still unclear how much each of them contributes, because of their functional redundancy *in vivo*. The first one to be mentioned is DNA sequence, which was initially thought to be the only determinant for nucleosomal positions. For the DNA to wrap around the histone octamer it needs to undergo bending which is energetically supported if certain dinucleotides with favorable geometry are present with the approximately 10bp helical periodicity. Specifically, AA/TT, TA, and AT are more common where the minor groove of the DNA faces the histone surface. In contrast, GG, GC, and CG tend to occur approximately 5 bp away or in regions where the minor groove is oriented outward from the histone (Satchwell et al., 1986). This periodic pattern underlies the high affinity of the so-called Widom 601 synthetic nucleosome-positioning sequence (Chua et al., 2012; Lowary & Widom, 1998), which is widely used for *in vitro* experiments, and is used for this project as well. On the other hand, longer stretches of poly-AT present in NFRs at promoters disfavor nucleosome formation due to the intrinsic rigidity, and also recruitment of the RSC remodeling complex, which then actively displaces nucleosomes (Lorch et al., 2014).

The organization of arrays at promoters closely relates to transcriptional activity. Research on *D. melanogaster* cells revealed that nucleosome arrays exhibit the highest degree of regularity within silent domains and heterochromatin, while showing the greatest irregularity near active gene promoters and enhancers. A similar inverse relationship between nucleosome array organization and gene activity was also identified in human cells (Baldi et al., 2018; Lai et al., 2018). This way, array regularity could contribute to the establishment of an inactive state at its very base. In terms of phasing, yeast promoter-proximal arrays can be assembled *in vitro* without general transcription factors or transcription (Krietenstein et al., 2016). Additionally, blocking RNA polymerase II does not largely influence promoter phasing *in vivo* (Weiner et al., 2010). However, transcription plays a role in the re-establishment of TSS arrays following replication (Vasseur et al., 2016) and is crucial for recruiting nucleosome remodelers to actively transcribed gene bodies (Smolle et al., 2012). Together, evidence suggests that transcription induces transient disturbances to the array structure, which is then counteracted by remodelers, which

reset the order. Notably, in *Drosophila* highly expressed genes tend to have less regular spacing (and shorter linker DNA) compared to silent genes, which maintain more evenly spaced nucleosomes (Baldi et al., 2018). This suggests that in silent regions, arrays remain stable and well-ordered, one of the reasons being the lack of disruptive transcriptional activity.

1.2.2 Chromatin remodeling

The nucleosome landscape is under constant stress from disruptive processes such as DNA replication, transcription and repair. Crucial factors that help reestablish the nucleosomal density and spacing are chromatin remodeling enzymes, which are believed to override DNA sequence-encoded positioning instructions. Although diverse in protein composition, all four major classes of remodelers have a similar ATPase motor domains that translocates DNA from a common location within the nucleosome, which breaks histone–DNA contacts (Clapier et al., 2017). Targeted by transcription factors and/or histone PTMs their activities can lead to various outcomes often referred to as either nucleosome assembly, chromatin access or nucleosome editing with the first one being the most relevant for this work as it encompasses the establishment of nucleosomal spacing. The SWI/SNF family of remodelers act on promoters to evict or slide away fragile nucleosomes, which together with general transcription factors generates an NFR and helps to position the +1 nucleosome (Kubik et al., 2019). ISWI and Chd1 remodelers are known to promote nucleosome assembly and the formation of regular nucleosome arrays *in vitro*. They can reposition nucleosomes from the ends of short DNA fragments toward the center, which reflects their role in nucleosome spacing (Stockdale et al., 2006; Torigoe et al., 2013; Tsukiyama et al., 1999). Supporting this, these remodelers enhance the formation of phased, regularly spaced arrays when acting on irregular nucleosome patterns generated *in vitro* (Oberbeckmann et al., 2021; Ocampo et al., 2016). Deletions experiments showed that ISWI and Chd1 remodelers space nucleosomes *in vivo* as well (Ocampo et al., 2016, 2019), moreover, outcome of the ISWI sliding activity appeared to be highly dependent on nucleosome density within regulatory domains (Abdulhay et al., 2023). Functionally similar remodeler INO80 also moves nucleosomes towards the center of the DNA when provided with long enough extranucleosomal DNA to facilitate sliding and setting regular spacing (Udugama et al., 2011), but it also shows an ability to position +1 nucleosomes to set the boundary of NFRs (Krietenstein et al., 2016; Singh et al., 2021).

Histone PTMs can play an important role in recruiting chromatin remodelers. As examples, human CHD1 contain chromodomains which bind H3K4me3 (Sims et al., 2005), RSC and SWI/SNF complexes contain bromodomains and their binding to chromatin is acetylation-sensitive (Chatterjee et al., 2011). Yeast ISW1b contains a PWWP domain and is recruited to active gene bodies marked by H3K36me3 (Smolle et al., 2012). As another example, the sliding activity of Chd1 is stimulated by ubiquitinated H2B (et al., 2016).

There are currently two proposed models for remodeler spacing mechanisms: the allosteric and the protein ruler model. In the allosteric model, the length of linker DNA is sensed by remodelers, which then slide nucleosomes preferentially towards the longer linker, which over enough time produces equal linkers. Produced internucleosomal distances are in this case dependent on nucleosome density (Yang et al., 2006). The other model builds on the fact that various remodelers have structural elements called protein rulers which extend a fixed distance from the nucleosome surface. When the ruler contacts a barrier, a DNA-bound factor like Reb1 or a neighboring nucleosome, steric hindrance disfavors further sliding towards the barrier but does not impede sliding away. The same reach and directional bias apply irrespectively of nucleosomal densities, therefore remodelers “clamp” nucleosomes together at fixed ruler-determined spacing (Oberbeckmann et al., 2021).

Altogether, a multistep model of regular array biogenesis emerges (Singh et al., 2021; Singh & Mueller-Planitz, 2021), in which Pol II transcription, replication and DNA damage are disruptive to the array regularity. DNA sequence exerts a bias for rough nucleosome positions, for example creating fragile unstable nucleosomes in regions that will become future NFRs. In yeast, general transcription factors (GTFs) together with SWI/SNF family remodelers (RSC, SWI/SNF) promote further nucleosome depletion at promoters by sliding and eviction (Kubik et al., 2019). Thirdly, the remodelers push the +1 nucleosome against existing barriers (Oberbeckmann et al., 2021) and away from its highest affinity further into the gene body. There could be a tug-of-war between RSC and INO80/ISW2 activities, which further sharpens the +1 nucleosome position (Kubik et al., 2019). Sliding activity of ISWI1 and Chd1 remodelers then promote regular array formation. These evenly spaced nucleosomal arrays are phased in respect to the TSS.

1.2.3 DNA Binders and Histone Variants

In yeast, remodelers work in conjunction with non-histone DNA binders. These provide barriers for proper nucleosome alignment at regions, which are supposed to remain depleted of nucleosomes. For example, origin recognition complexes occupy replication origins or general transcription factors bind to the promoter regions (Eaton et al., 2010; Kubik et al., 2018). Consistently, when these factors are depleted, the regular phased arrays shift towards their binding sites (Krietenstein et al., 2016). Similarly, in higher organisms phased regular arrays mark binding sites of several transcription factors. The binding of mammalian transcription factor CTCF, which is known to be responsible for setting and insulating chromatin boundaries, mirrors the degree of array regularity – the higher the genomic occupancy of CTCF at particular sites, the higher the NRL and regularity of proximal nucleosomal arrays (Clarkson et al., 2019). Interestingly, patients with chronic lymphocytic leukemia have both significant changes in global nucleosome positioning and also disrupted binding of these 3D chromatin organizers including CTCF, possibly highlighting the importance of spacing in proper epigenetic regulation (Piroeva et al., 2023).

The role of a nucleosome can be modulated by incorporating various non-canonical histone variants, which are typically located in specific genomic regions and contribute to regulation, identity, chromatin packaging and nucleosome stability of those specific regions. Differences in nucleosome composition have been shown to affect nucleosomal arrays architecture. Moreover, the presence of H2A.Z histone variant in nucleosomes can affect the sliding activity of INO80, which selectively exchanges H2A.Z-H2B dimers for canonical dimers as it translocates along nucleosomal DNA (Brahma et al., 2017). Similarly, the ISWI family of chromatin remodelers showed an increase in activity on nucleosomes that include the H2A.Z variant (Goldman et al., 2010). Arrays containing the H2A.Bbd variant have a decreased nucleosomal repeat length and bind DNA less tightly in comparison to arrays with canonical nucleosomes (Tolstorukov et al., 2012).

Increasing the complexity, another important player is the linker histone H1. It binds by the exit and entry sites of nucleosomal DNA (**Figure 1**) and is important for higher-order structure stabilization. In higher organisms, H1 knockdown caused a strong shift in NRL towards shorter linkers and loss of regularity resulting in a more open chromatin state (Baldi et al., 2018). Naturally coexisting H1 subtypes even have varying effects on NRL

possibly pointing to their distinct role in organization of chromatin domains (Öberg et al., 2012).

1.3 Biology of Nucleosomal Arrays and Spacing

Even though there has been more information emerging on the biogenesis of these regularly spaced arrays, the functional side of this is still lacking and the precise biological roles are less known. The complex 3D organization of chromatin - its establishment, maintenance and dynamic regulation - is highly dependent on internucleosomal spacing. The spacing regulation is closely related to the key aspect of accessibility to chromatin binders, cryptic transcription prevention, protection against DNA damage repair and others discussed below.

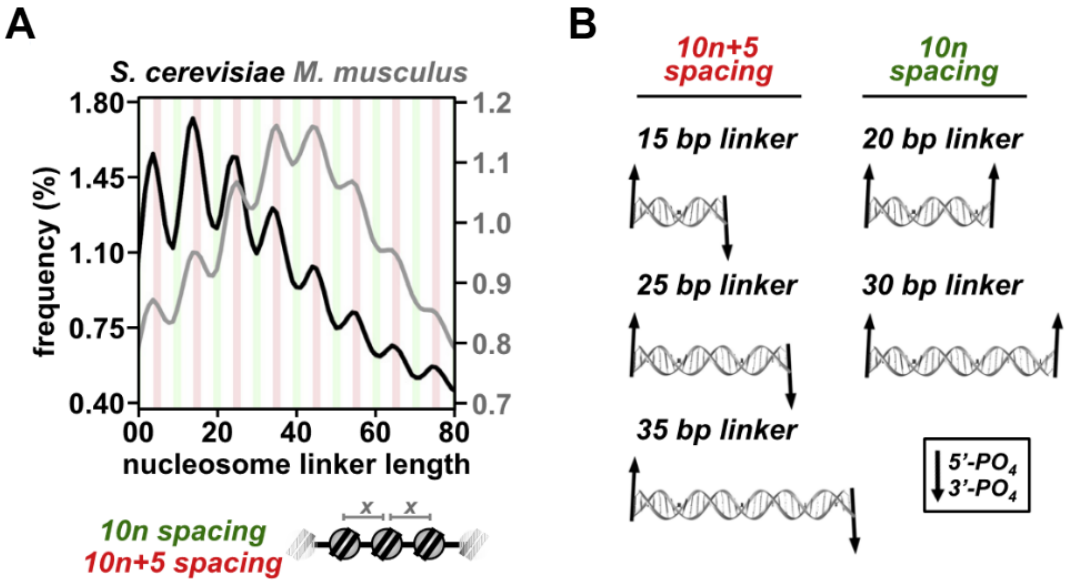

Figure 3. Linker DNA quantization patterns. (A) In yeast (black) and mouse embryonic stem cells (grey), linker lengths are biased towards 10n+5 and depleted for 10n base pairs. **(B)** End orientation trajectories of B-form DNA with 10n+5 and 10n bp. Since a full turn takes ~10 bp, 10n+5 linkers result in an ~180° difference in the orientation of DNA ends (and nucleosomes) disfavoring stacking found in 30nm fiber structures. On the other hand, 10n linkers enable the nucleosomes to engage in face-to-face stacking interaction found in 30nm fibers. Adapted from Gibson et al., 2019.

1.3.1 Prevention of Cryptic Transcription

Regular nucleosome arrays, maintained by chromatin remodelers such as ISWI and CHD1, are vital for preventing transcription from cryptic promoters within gene bodies (marked with histone H3 lysine 36 methylation) during transcriptional elongation. They ensure that potential cryptic promoters remain inaccessible, thereby preserving the integrity of gene expression. Loss of these remodelers disrupts regular arrays, which leads to

increased chromatin accessibility and aberrant transcription initiation from both sense and antisense strands (Hennig et al., 2012; Pointner et al., 2012; Smolle et al., 2012). Remodelers interact with histone modification pathways. For instance, the Set2-Rpd3S pathway, which involves histone H3 lysine 36 methylation and subsequent deacetylation, works in concert with chromatin remodelers to maintain a repressive chromatin environment within gene bodies. Disruption of this pathway, along with the loss of chromatin remodelers leads to accumulation of aberrant transcripts (Hennig et al., 2012).

1.3.2 Protection against DNA Damage and Repair

Nucleosome wrapping itself protects the underlying DNA against breaks induced by ionizing radiation and reactive oxygen species (Brambilla et al., 2020). Consistently, cells with functional remodelers that have the capacity to generate regularly spaced arrays are more resistant to genotoxic stress induced by various physical and chemical DNA-damaging agents (Singh et al., 2021). On top of that, arrays generated by ISWI and Chd1 create even coating, which was proposed to expose less accessible DNA for ectopic recombination and integration of mobile elements (Singh et al., 2021).

1.3.3 Higher Order Structure Formation

It is important to note that nucleosomal arrays are not linear, but function in the complex 3D nuclear environment. Chromatin compartmentalizes via multivalent interactions within and between fibers setting the base for liquid-liquid phase separation (LLPS) behavior. This behavior is modulated by internucleosomal spacing. The propensity of chromatin to form phase separated droplets is higher for chromatin fibers that follow the more prevalent 10n+5 spacing pattern (e.g. 15, 25bp linkers) compared to those with 10n (e.g. 20, 30bp linkers). Arrays with 10n+5 spacing phase separate at lower salt concentrations forming droplets of higher chromatin concentration (Gibson et al., 2019). Chromatin primary fiber forms higher order structures, but the regulation and extent remain unclear. The highly debated 30nm chromatin fiber may form *in vitro* under specific ionic strength conditions, but there is little evidence for the existence of extensive compact regular fibers *in vivo*. Instead, *in situ* cryo-ET studies show that chromatin likely exists as a flexible zig-zag polymer, allowing greater regulatory potential and having the ability to undergo a 30nm fiber-like structural change locally and transiently in regions with shorter NRLs that are typical for transcriptionally active regions of chromatin (Correll et al., 2012; Hou et al., 2023). Linkers, however, play a crucial role in local fiber folding as it is a property highly

dependent on nucleosomal stacking interactions and the spatial organization of linker DNA. Simulations and force spectroscopy experiments showed a 10bp periodical change in stacking preferences and fiber stability with increasing linker length – stacking is most stable when linkers are multiples of 10 bp due to optimal helical phasing. Longer linkers (45-55 bp) distribute mechanical stress from stacking more evenly than shorter linkers (20-30 bp) (Bass et al., 2019; Brouwer et al., 2021). Since canonical DNA (B form) needs ~10 bp for a helical turn, nucleosomes connected by a 10n linkers are separated by approximately an integral number of turns. The resulting orientation enables face-to-face stacking of first and third nucleosomes in an array (**Figure 3B**), which allows the 30nm fiber to form (Brouwer et al., 2021; Correll et al., 2012). On the other hand, nucleosomes connected by 10n+5 linkers are rotated away from each other by 180° forming a configuration that does not favor regular higher-order structures (Robinson et al., 2006). Studies of arrays with linkers spanning 10n and 10n+5 bp point at a periodic relationship, where linker lengths approaching 10n bp afford more compact, regular, and energetically stable fibers (Brouwer et al., 2021; Correll et al., 2012).

A recent study by Chen et al. (2025) combines biochemistry and multiscale simulations demonstrates that the propensity for phase separation changes also within the 10n to 10n+5 interval (e.g. 25-30 bp) (**Figure 4A**). Single-bp increments in linker length caused shifts in thresholds for LLPS and dynamics within droplets with a sharp transition between 27 and 28 bp. The simulations explained this as a balance between intra-fiber and inter-fiber nucleosome interactions – shorter linkers hinder intra-fiber stacking and expose nucleosome faces, that can engage in strong multivalent inter-fiber contacts that favor LLPS (**Figure 4B**). Opposingly, longer linkers within this interval promote stable intra-fiber stacking interactions, which reduces intermolecular binding and accelerates droplet dynamics. In the same study, authors showed how nucleosome remodeling by ISWI can regulate condensation by altering the length of linker DNA. Using chromatin arrays with 25 or 30bp linkers and defined segments of free DNA on ends of arrays, it was demonstrated that ISWI shifts spacing towards predicted lengths that either promoted LLPS (30→35 bp) or disfavored it (25→30 bp). Altogether, it appears that even slight changes in length and torsional constraints of linker DNA significantly alter the chromatin stacking and condensation.

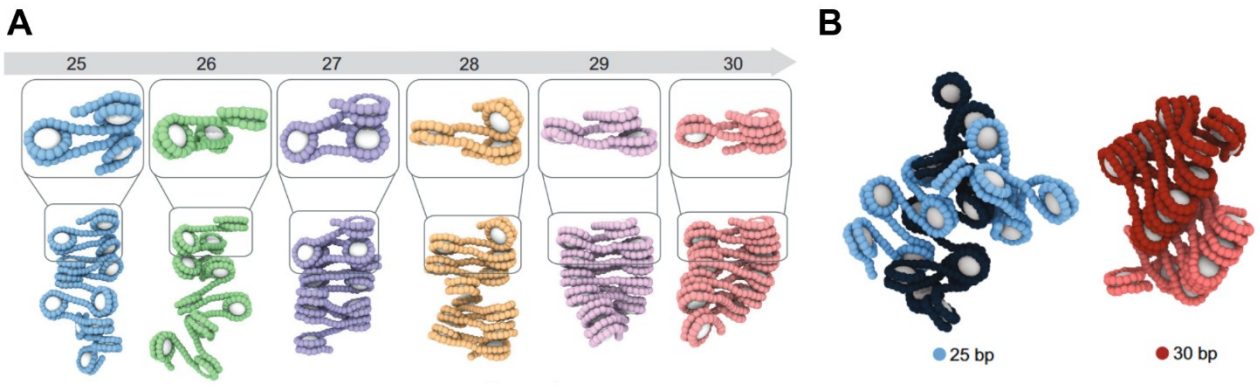

Figure 4. Linker length influence on chromatin fiber structure. (A) Structures of 12-nucleosomal arrays from coarse-grained simulations inside the condensed phase. As linker length approaches 30 bp (red), representing 10n spacing, nucleosomes engage more in face-to-face stacking typical for 30nm fiber structure. In contrast, as the linker length decreases towards 25 bp (blue) (10n+5) arrays are folded unevenly with little intra-fiber stacking. **(B)** Snapshots from simulations of inter-fiber interactions: 30bp linker arrays (red) engage in more face-to-face interactions within the same fiber in comparison with 25bp arrays, which preferentially form heterogenous contacts with neighboring fibers. Adapted from Chen et al., 2025.

1.3.4 Enhancer-Promoter Communication

In higher organisms, active enhancers have the regular array organization and its NRL may affect the communication between enhancers and promoters. The presence of nucleosome-free gaps in arrays decreases the rate of enhancer-promoter communication. Additionally, increasing NRL resulted in increased rates of enhancer-promoter communication by both modulating the overall structure and flexibility mainly in actively transcribed regions and their regulatory elements (Nizovtseva et al., 2017).

1.4 Aims of the Project

Understanding how chromatin structure influences protein binding is central to decoding the complex regulatory mechanism of all DNA-related processes, including transcription of underlying genes. Internucleosomal spacing defined by variable DNA linker length could play a crucial role in tuning DNA accessibility, defining spatial reach of binders, or locally altering the 3D architecture. Constructing nucleosomal arrays with defined linker lengths within relevant ranges and subjecting them to proteomic profiling could lead to identification of chromatin-associated factors whose binding is sensitive to nucleosome spacing. Differential analysis of proteomic profiles for different defined linkers offers a powerful way to systematically study how structural features of chromatin contribute to

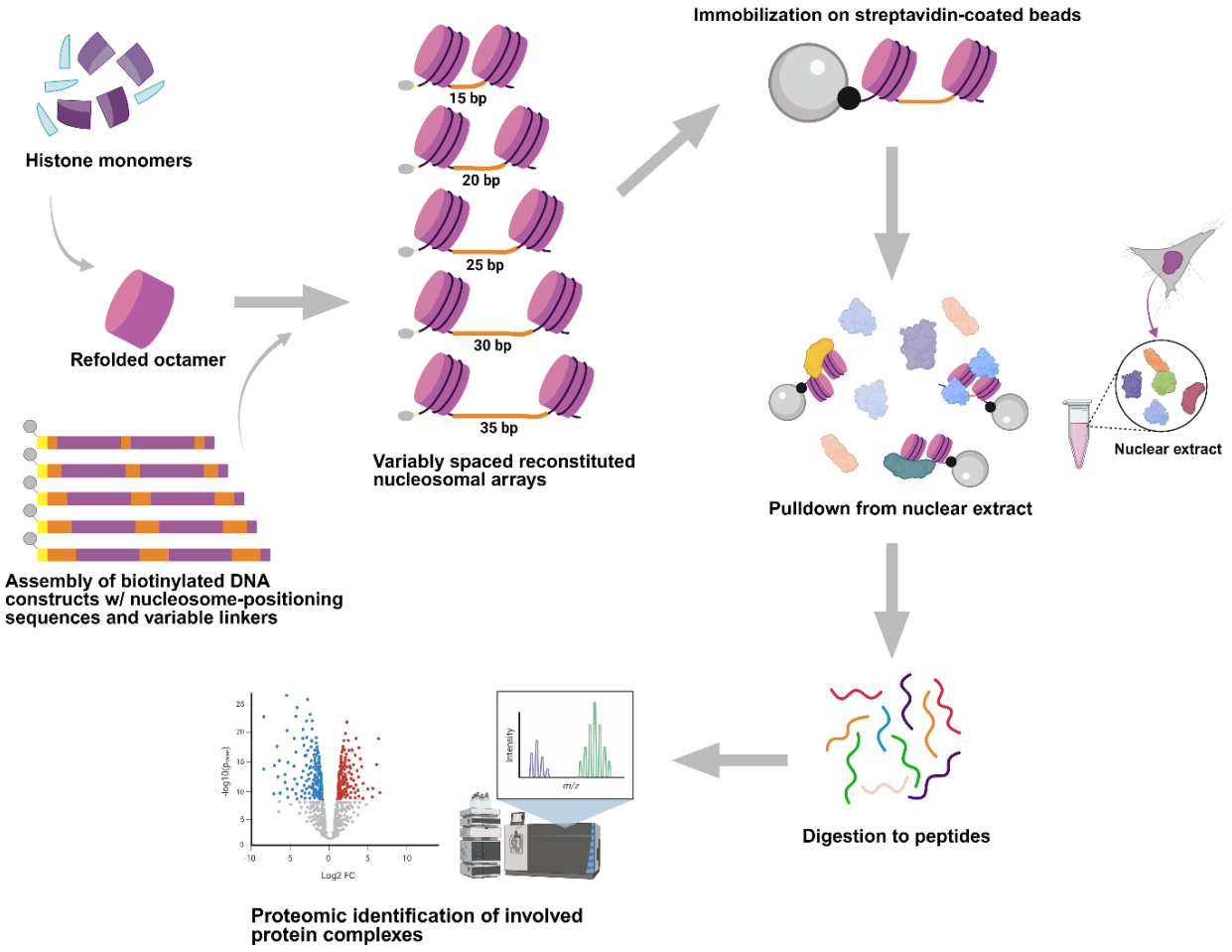

Figure 5. **Design of this study.** A library of variously spaced high-affinity nucleosome-positioning sequences is constructed within plasmid vectors and subsequently isolated and terminally labeled with biotin. Octamers of native histone proteins are refolded from monomers and combined with DNA constructs to reconstitute nucleosomes with linker DNA of variable length. The terminal biotin label then serves for immobilization on streptavidin-coated magnetic beads. Immobilized nucleosomes work as a bait for a subsequent pulldown experiment from isolated nuclear lysates. Fished out proteins are fragmented and analyzed using mass spectrometry.

the selective recruitment of regulatory complexes, and whether spacing by itself can serve as a discriminatory signal irrespectively of the histone code.

The primary objectives of this project include:

- Development of a methodological pipeline (summarized in **Figure 5**) for the reconstitution of chromatin arrays with precisely controlled nucleosome spacing.
- Design and construction of a library of DNA constructs with strong nucleosome-positioning sequences and defined linker lengths.

- Production of DNA constructs in substantial quantities within plasmids and isolating them from plasmid backbone DNA.
- Design of a labeling strategy to enable immobilization on beads.
- Reconstitution of nucleosomal arrays that can serve as a bait for affinity purification mass spectrometry experiments.

This multi-step approach presents several technical challenges, including maintaining the integrity and homogeneity of the DNA templates, achieving efficient biotinylation and reproducible nucleosome assembly to ensure specific and sensitive proteomic analyses. Establishing this pipeline could hold potential to decipher how nucleosome spacing influences the recruitment of chromatin-associated factors in a controlled *in vitro* setting.

2 Materials and Methods

2.1 Materials

If not listed below in **Table 1**, routine chemicals were purchased from Sigma-Aldrich in quality suitable for molecular biology.

Table 1. Reagents and materials used throughout this project.

	Material	Source	Product Code
Reagents	0,2% EDTA with phenol red	IMG	-
	1x TBS with 1% casein	Bio-Rad	1610782
	40% acrylamide/bis, 29:1	Bio-Rad	1610146
	acetic acid	Lach-Ner	10047-C98-M1000-1
	acrylamide	Sigma-Aldrich	A8887
	agarose	Amresco	0710-500G
	ampicillin	BB Pharma	8588001339104
	Anti-Anti	Thermo Fisher	15240062
	biotin -11-dUTP	Thermo Fisher	R0081
	Bovine Serum Albumin	Sigma-Aldrich	A3803
	chloroform : isoamyl alcohol 24:1	Sigma-Aldrich	C0549
	CutSmart buffer	NEB	B7204S
	dATP	NEB	N0440S
	dNTP mix	NEB	N0447L
	ethanol	Lach-Ner	20025-A96-M2500-1
	Fetal Bovine Serum (FBS)	Sigma-Aldrich	F7524
	Gel Loading Dye, Purple (6X)	NEB	B7024S
	GelRed	Biotium	41003

	GlutaMAX	Thermo Fisher	35050061
	glycerol	Penta Chemicals	14530-11000PE
	isopropanol	Lach-Ner	20037-CT0-M2500-1
	N,N'-methylene bisacrylamide	Roth	7867.1
	NEB2 buffer	NEB	B7002S
	phenol	Roth	0038.3
	Phusion HF Buffer	NEB	B0518S
	potassium acetate	Thermo Fisher	A16321.0E
	potassium chloride	Penta Chemicals	16200-31000
	SimplyBlue SafeStain	Thermo Fisher	LC6065
	T4 ligase buffer	NEB	B0202S
	TCEP	Merck	580560
Kits	Protein Assay Kit II	Bio-Rad	5000002
	DNA Clean & Concentrator-5	Zymo Research	D4004
	NucleoSpin Gel and PCR Clean-up	Macherey-Nagel	740609.5
	NucleoSpin Plasmid DNA	Macherey-Nagel	12353358
Media	DMEM	Sigma-Aldrich	D1145
	LB broth (Lennox)	Sigma-Aldrich	L3022
	LB Broth with agar (Lennox)	Sigma-Aldrich	L2897
	Terrific Broth (TB)	Roth	X972.1
Enzymes	EcoRI-HF	NEB	R3101M
	BamHI-HF	NEB	R3136S
	DpnI	NEB	R0176L
	HindIII-HF	NEB	R3104M
	Klenow fragment	NEB	M0210L
	Lysozyme	Sigma-Aldrich	L6876
	Mnase	NEB	M0247S
	Phusion-HF DNA Polymerase	NEB	M0530L
	Quick CIP	NEB	M0525S
	RNAse A	Worthington	LS005649
	rSAP	NEB	M0371S
	SmaI	NEB	R0141L
	T4 DNA Ligase	NEB	M0202M
	T5 Exonuclease	NEB	M0363L
	Taq DNA Ligase	NEB	M0208L
	Trypsin	Thermo Fisher	15090046
Cells	HEK 293	ATCC	CRL-1573
	NEB 5-alpha Competent E. coli	NEB	C2987I
Antibodies	AzureSpectra Goat-anti-rabbit IgG IR800	Azure Biosystems	SKU AC2134
	AzureSpectra Goat-anti-mouse IgG IR700	Azure Biosystems	SKU AC2129
	Histone H3 (D1H2) XP Rabbit mAb	Cell Signaling Technology	4499S
	α-Tubulin (DM1A) Mouse mAb	Cell Signaling Technology	3873S

Others	Amicon Ultra Centrifugal Filter (10kDa MWCO)	Merck	UFC9010
	Dynabeads M-280 Streptavidin	Thermo Fisher	11206D
	GeneRuler DNA ladder	Thermo Fisher	SM0333
	MagRack 6	Cytiva	28948964
	MonoQ 5/50 GL	Cytiva	17-5166-01
	mPAGE 4-20% Bis-Tris Precast Gels	Merck	MP42G15
	Precision Plus Protein™ All Blue Prestained Protein Standards	Bio-Rad	1610373
	Protease Inhibitor Cocktail	Roche	11836170001
	Protein LoBind Tubes	Eppendorf	30108116
	Quick-Load Purple 100bp DNA ladder	NEB	N0551S
	Quick-Load Purple 1kb DNA ladder	NEB	N0550S
	Slide-A-Lyzer MINI Dialysis Cups (10kDa MWCO)	Thermo Fisher	PI69570
	Spectra BR Protein Ladder	Thermo Fisher	26634
	Superdex 200 Increase 10/300 GL	Cytiva	28990944
	Tissue culture dish 100	TPP	93100
	Tissue culture dish 150	TPP	93150
	Dialysis membrane Spectra/Por 7 (10kDa MWCO)	Repligen	E870.1
Software	SnapGene 8.1		
	Cytiva Unicorn 7		
	BioRender		
	Magellan Standard		
	UniProt DB		
	GraphPad Prism 10		
	MS Excel		

Table 2. Composition of used buffers

Buffer Name	Composition (1× concentration)
AE buffer A	50 mM Tris-HCl, 0.5 mM EDTA, pH 8.0
AE buffer B1	50 mM Tris-HCl, 0.5 mM EDTA, 1 M NaCl, pH 8.0
AE buffer B2	50 mM Tris-HCl, 0.5 mM EDTA, 2 M NaCl, pH 8.0
Annealing Buffer	10 mM Tris-HCl pH 7.5, 50 mM NaCl, 1 mM EDTA
Buffer P1	50 mM Tris-HCl, pH 8.0, 10 mM EDTA
Buffer P2	200 mM NaOH, 1% SDS
Buffer P3	3M Potassium acetate, pH 5.5 (adjusted w/ acetic acid)

BW Buffer	2 mM Tris-HCl, pH 7.5, 1 mM EDTA, 1 mM DTT, 150 mM NaCl
CutSmart (NEB)	50 mM potassium acetate, 20 mM Tris-acetate, 10 mM magnesium acetate, 100 µg/ml BSA, pH 7.9
Dilution Buffer	10 mM Tris-HCl, pH 8.0
DNA Buffer	50 mM Tris-HCl, 0.5 mM EDTA, pH 8.0
Fractionation Buffer A (FBA)	20 mM Tris-HCl pH 7.5, 10 mM KCl, 1.5 mM $MgCl_2$, 10% glycerol, 1× protease inhibitor cocktail
Isothermal Reaction Buffer (IAB)	100 mM Tris-HCl (pH 7.4), 10mM $MgCl_2$, 0.2 mM each dNTP, 10 mM DTT, 5% (v/v) PEG 8000, 1 mM NAD
MNase Buffer (MNB)	10 mM Tris-HCl pH 7.6, 15 mM NaCl, 60 mM KCl, 0.1% Igepal CA-630, 1× protease inhibitor cocktail, 10 mM sodium butyrate
MOPS running buffer	50 mM Tris, 50 mM MOPS, 0.1% (w/v) SDS, 1 mM EDTA
Nuclear Buffer B (NBB)	20 mM Tris-HCl pH 7.5, 150 mM NaCl, 1.5 mM $MgCl_2$, 10% glycerol, 1× protease inhibitor cocktail
Nuclear Buffer C (NBC)	30 mM HEPES pH 7.8, 300 mM NaCl, 0.1% Igepal CA-630, 20% glycerol, 0.4 mM EDTA, 1× protease inhibitor cocktail, 10 mM sodium butyrate
PBS	137 mM NaCl, 2.7 mM KCl, 4.9 mM Na_2HPO_4, 13.4 mM KH_2PO_4
RB High	10 mM Tris (pH 7.5), 2 M KCl, 1 mM EDTA, 1 mM DTT
RB Low	10 mM Tris-HCl, pH 7.5, 250 mM KCl, 1 mM EDTA, 1 mM DTT
Refolding Buffer	10 mM Tris-HCl (pH 7.5), 2 M NaCl, 1 mM EDTA, 5 mM β-mercaptoethanol
SDS-PAGE Sample Buffer	62.5 mM Tris-HCl pH 6.8, 1.5% (w/v) SDS, 8.3% (v/v) glycerol, 0.005% (w/v) bromophenol blue, 1.5% (v/v) 2-mercaptoethanol
T4 Ligase Buffer (NEB)	50 mM Tris-HCl, 10mM $MgCl_2$, 1 mM ATP, 10 mM DTT, pH 7.5
TAE	40 mM Tris, 20 mM acetic acid, 1 mM EDTA (pH 8.3)
TBE	9 mM Tris, 89 mM boric acid, 2 mM EDTA (pH 8.3)
TBS	150 mM NaCl, 50 mM Tris-HCl, pH 7.6
TBST	20 mM Tris, 150 mM NaCl, 0.1% (w/v) Tween
TCS	20 mM Tris-HCl, pH 7.5, 1 mM EDTA, 1 mM DTT
Unfolding Buffer	6 M guanidine hydrochloride, 20 mM Tris-HCl (pH 7.5), 5 mM DTT

2.2 Gibson Assembly Master Mix Preparation

To prepare the Gibson Assembly Master Mix for the heavily used isothermal assembly of DNA fragments, first 6 mL of 5× Isothermal Reaction Buffer (IAB) was prepared on ice according to **Table 3**. The mixture was then rotated at 4°C to dissolve PEG into solution. The mixture was then split into 320 ul aliquots.

Table 3. Preparation of Isothermal Reaction Buffer (IAB) for the Gibson Assembly Master Mix

Component	Stock Conc.	Volume Used	Final conc. in mL (5×)	Final conc. in 1×
Tris-HCl (pH 7.4)	*1 M*	*3.0 mL*	*500 mM*	*100 mM*
$MgCl_2$	*1 M*	*0.3 mL*	*50 mM*	*10 mM*
dNTPs (each)	*100 mM*	*60 µL each*	*1 mM each*	*0.2 mM*
DTT	*1 M*	*0.3 mL*	*50 mM*	*10 mM*
PEG-8000	*solid*	*1.5 g in 6 mL*	*~25% (w/v)*	*5% (w/v)*
NAD	*50 mM*	*0.6 mL*	*5 mM*	*1 mM*

To one aliquot of 5× IAB buffer T5 Exonuclease, Phusion polymerase, Taq ligase (all from NEB) and nuclease-free water were added according to **Table 4**, which brought the concentration of the Master Mix to 1.33×. The mixture was split into 15ul aliquots that are supposed to be filled up with DNA fragments and water to 20 ul and therefore dilute the Master Mix to 1×.

Table 4. Enzymes contained in the Gibson Assembly Master Mix.

Component	Stock concentration (U/µL)	Volume per 320 µL of 5× IAB (µL)
T5 Exonuclease (NEB M0363L)	*10*	*1.2*
Taq DNA Ligase (NEB M0208L)	*40*	*160*
Phusion-HF DNA Polymerase (NEB M0530L)	*2*	*20*
nuclease-free water	*-*	*to 1.2 mL*

2.3 Linker Expansion

Colleague Dr. Michal Svoboda kindly provided Plasmid DNA (pUC19), which carried a single Widom 601 repeat flanked by a 5′ linker of 15 or 30 bp. To extend the linker by 5 bp, a 35µL polymerase chain reaction (PCR) reaction was assembled on ice and contained 1× Phusion HF buffer (NEB), 200 µM dNTPs, 0.5 µM of each primer (sequences listed in **Supplementary Table**), 50 ng of pUC19 template DNA, 0.7 U of Phusion DNA

Polymerase (NEB), and nuclease-free water. Reaction was mixed, spun quickly and transferred to a thermocycler (Biometra T3) preheated to 98 °C. The thermocycling conditions are described in **Table 5**. PCR products were analyzed via agarose gel electrophoresis (0.7% agarose in 1× TAE buffer, 100 V, 45 min) and stained with GelRed (Biotium). To remove methylated template DNA, 20 U of DpnI (NEB) were added to the reaction and incubated at 37 °C for 1 hour. The amplified DNA was purified using the DNA Clean & Concentrator-5 Kit (DCC kit, Zymo Research).

Table 5. **Thermocycling conditions used for PCR-based steps of 1×Widom construct assembly.**

Step		Temperature (°C)	Time
Initial denaturation		*98*	*30 s*
	Denaturation	*98*	*10 s*
30 cycles	*Annealing*	*62*	*30 s*
	Polymerization	*72*	*60 s*
Final extension		*72*	*10 min*
Hold		*4*	

A single-fragment Gibson Assembly reaction was set up on ice, consisting of 50 ng of the PCR product, 1× Gibson Assembly Master Mix, and nuclease-free water to a total volume of 20 µL. The mixture was incubated at 50 °C for 30 minutes. The assembled product was diluted 4 times, and 4 µL of the mixture were transformed into chemically competent *E. coli* (NEB 5-alpha) cells by heat shock and incubated in LB medium for 30 minutes at 37 °C with shaking. Cells were plated onto LB agar plates supplemented with 100 µg/mL ampicillin and incubated overnight at 37 °C.

Several colonies were picked and inoculated into 2 mL of LB medium with ampicillin. After overnight growth at 37 °C, cells were pelleted (4,000×g, 10 min, 4 °C) and plasmid DNA was isolated using the NucleoSpin Plasmid Mini Kit (Macherey-Nagel). DNA concentration and purity were assessed spectrophotometrically using NanoDrop One (Thermo Scientific). To confirm the success of cloning, 500 ng of plasmid DNA were mixed with M13 primers, filled up to 10 µL with water, and submitted for Sanger sequencing (SeqMe).

The verified plasmid containing the 1× Widom 20 or 35 bp linker insert was used as a template for a second round of PCR (UniLF and Vet_ot_Rlong primers, **Supplementary table**). The PCR was assembled as previously described, using 50 ng of the new template

and an annealing temperature of 61 °C. PCR products were analyzed via 0.7% agarose gel electrophoresis, digested with DpnI, and purified as described above.

To add the second linker, single-stranded oligonucleotides (**Supplementary table**) were annealed in 1× Annealing Buffer (10 mM Tris-HCl pH 7.5, 50 mM NaCl, 1 mM EDTA) at 25 µM each in a total volume of 50 µL. Annealing was performed in a thermocycler as presented in **Table 6**.

Table 6. Conditions used for annealing single-stranded oligonucleotides.

Step	Temperature (°C)	Time (min)
Initial denaturation	*95*	*5*
Linear ramp	*95 → 27*	*60*
Hold	*27*	*20*

The resulting double-stranded oligonucleotide was inserted into the PCR product from the previous step using Gibson Assembly at a 5:1 insert-to-vector molar ratio (50 ng vector, 12 ng insert) in a total volume of 10 µL. A negative control containing only the vector was included. Reactions were incubated at 50 °C for 30 minutes, then transformed into competent *E. coli* cells as described above. Colonies were screened via Sanger sequencing using M13 primers. The same full process was performed similarly to prepare a single Widom 20bp linker construct from a 15bp linker 1×Widom precursor, except with corresponding primers listed in **Supplementary Table**. The other constructs (1×Widom with 15, 25 and 30bp linkers) were assembled by Dr. Michal Svoboda.

2.4 Propagation of Widom repeats

For propagation of plasmid DNA containing N× Widom flanked by variable linkers, 1 µg of plasmid was digested with 100 U of HindIII-HF (NEB) in 1× CutSmart buffer (NEB) and incubated at 37 °C overnight. To prevent vector re-ligation, the open plasmid was dephosphorylated with 1 U of recombinant Shrimp Alkaline Phosphatase (rSAP, NEB) for 60 minutes at 37 °C. The resulting linearized vector was purified using the DNA Clean & Concentrator-5 Kit (Zymo Research). In parallel, 5 µg of plasmid DNA were double-digested with 150 U of EcoRI-HF (NEB) and 30 U BamHI-HF (NEB) in 1× CutSmart buffer and incubated overnight at 37 °C. The digested insert was separated from the vector by preparative agarose gel electrophoresis (1.5% agarose in 1× TBE, 90 V, 60 min), excised,

and extracted using the NucleoSpin Plasmid Gel Extraction Kit (Macherey-Nagel). The fragment was further purified with the DNA Clean & Concentrator kit, and DNA concentration was determined by NanoDrop. Assembly of the insert and vector was performed using Gibson Assembly at a 4:1 molar ratio (50 ng vector) in 20µL reactions using 1× Gibson Master Mix. The mixture was incubated, diluted, and transformed into competent *E. coli* as described previously. Colonies were screened by sequencing to confirm correct seamless multimer assembly. The full 2D library of Widom constructs was prepared employing this procedure.

2.5 Large-scale Plasmid Production

2.5.1 Bacterial Culture

Plasmid DNA was prepared from *E. coli* (NEB 5-alpha) cells transformed with the desired plasmid construct. Transformed colonies were first inoculated into 50 ml of sterilized Terrific Broth medium (TB, Roth) supplemented with 100 µg/ml ampicillin (BB Pharma) and 4 mL/L glycerol. The starter culture grew for at least 8 hours or overnight at 37 °C with shaking and used to inoculate 1.5 L volumes of the same medium (25 mL starter per 1.5 L TB) with few drops of antifoam. Culture grew overnight at 37 °C with aeration using the LEX bioreactor (Epiphyte3). Cells were harvested by centrifugation (8000 × g, 10 min, 4 °C) and washed with PBS. The resulting pellets were stored at –80 °C.

2.5.2 Plasmid Purification

Cell pellet was resuspended in Buffer P1 (50 mM Tris-HCl, pH 8.0, 10 mM EDTA, 15 mL per 1 g of pellet). Lysozyme (Sigma-Aldrich) and RNase A (Worthington) were added to 1 mg/mL and 0.1 mg/mL respectively, and the mixture was incubated for 30 min at 4 °C with occasional gentle mixing. An equal volume of Buffer P2 (200 mM NaOH, 1% SDS) was added, and the solution was gently inverted to lyse cells and ensure homogeneity. Immediately afterward, an equal volume of ice-cold Buffer P3 (3 M potassium acetate, pH 5.5) was added, followed by vigorous mixing to initiate precipitation of membranes and genomic DNA. The lysate was incubated on ice for 30 min and centrifuged (7000 × g for 30 min at 4 °C). The supernatant was collected and divided into 850 mL volumes in 1L centrifuge bottles. To each lysate, NaCl and PEG 6000 were added (1 M NaCl, 10% PEG). The solution was shaken at 37 °C to dissolve solids, then incubated at 4 °C overnight to precipitate plasmid DNA. The mixture was centrifuged at 12,000 × g for 1 hour at 4 °C.

Pellets were resuspended in 20–100 mL of DNA Buffer (50 mM Tris-HCl, 0.5 mM EDTA, pH 8.0). The resuspension was centrifuged at 20,000 × g for 20 min at room temperature, and the supernatant was kept. To remove proteins, lipids and SDS, the resuspended DNA was extracted twice with an equal volume of phenol (Roth) and twice with chloroform:isoamyl alcohol (24:1, Sigma-Aldrich). For each extraction, the mixture was vortexed for ~2 min and centrifuged at 16,000 × g for 10 min and the upper aqueous phase was carefully transferred to a clean tube after each step. To precipitate the final DNA at room temperature, NaCl (500 mM) and 0.7× volume of isopropanol was added. DNA was pelleted by centrifugation at 16,000 × g for 30 min, washed with 70% ethanol, and air-dried. The DNA was resuspended in 2–10 mL of DNA Buffer. DNA quality and size were assessed by agarose gel electrophoresis (1%, TAE buffer, GelRed stain) and concentration was determined spectrophotometrically.

2.6 Octamer Refolding

Lyophilized histone proteins (H3, H2A, H2B, H4 from *Xenopus laevis*, expressed and purified by Dr. Vanda Lux) were resuspended individually in Unfolding Buffer (6 M guanidine hydrochloride, 20 mM Tris-HCl (pH 7.5), 5 mM dithiothreitol (DTT)) to at least 2 mg/mL, typically in around 250 µL. Samples were incubated at room temperature for 1 hour to allow complete unfolding. Protein concentrations were determined spectrophotometrically by measuring absorbance at 280 nm against the Unfolding Buffer using NanoDrop. Each sample was measured in triplicate, and concentrations were calculated using the extinction coefficients of the respective histones. Histones were then combined in equimolar ratios to a final protein concentration of 1 mg/mL in Unfolding Buffer. A total of approximately 6 mg of histones were refolded at a time. The histone mixture was placed into a pre-wetted dialysis membrane with a molecular weight cut-off (MWCO) of 10 kDa (Repligen). The mixture was dialyzed against Refolding Buffer (10 mM Tris-HCl (pH 7.5), 2 M NaCl, 1 mM EDTA, 5 mM β-mercaptoethanol) at 4 °C. Dialysis was performed with 3 buffer exchanges – every 6 hours and the last step overnight. Following dialysis, the membrane was evacuated, and any precipitated material was removed by centrifugation. The solution was concentrated to a final volume of 200-500 µL using a centrifugal filter (Amicon, 10 kDa Molecular weight cut-off (MWCO)). Size exclusion chromatography was performed using a Superdex 200 Increase 10/300 column (Cytiva) and AKTA Pure 25 FPLC (Amersham Biosciences) with flow rate set to 0.75 mL/min and maximum pressure

over the column set to 2.6 MPa. Column was equilibrated in Refolding Buffer followed by manual sample loading and isocratic elution (1 CV). Fractions were analyzed by SDS-PAGE to confirm histone composition. Octamer-containing fractions were pooled and further concentrated using a 10 kDa MWCO centrifugal filter to no more than 15 mg/mL.

2.7 Nucleosome reconstitution

2.7.1 Stepwise Dilution Assembly

The assembly reaction was set up on ice in a total volume of 20 µL using DNA, histone octamers (both in kept in a buffer containing 2M NaCl) and RB high buffer (10 mM Tris (pH 7.5), 2 M KCl, 1 mM EDTA, 1 mM DTT). The histone:DNA ratio was set to 1:1 (5.56 µl of 10 µM stock DNA, 6.15 µl of 13 µM stock octamer, 8.29 µl of RB high). The mixture was incubated at room temperature for 30 minutes. The salt concentration was then sequentially decreased by stepwise addition of Dilution Buffer (10 mM Tris-HCl, pH 8.0) at room temperature. The reaction was brought to 1.48 M, 1.0 M, 0.6 M, 0.25 M NaCl with 30-minute incubations at room temperature after each step. Assembly efficiency was assessed using native gel electrophoresis. Polyacrylamide gel (5%, 0.2 x TBE buffer) was pre-run (100 V, 45 min), and then samples were loaded and run at room temperature. Band shifts were visualized using GelRed.

2.7.2 Gradient Dialysis Assembly

Small-scale reconstitutions were carried out in 20 µL volumes. DNA concentration was held constant while histone octamer concentration was varied slightly above and below a 1:1 molar ratio. All reconstitution steps were performed at room temperature. Buffers were freshly prepared. These included RB High buffer, RB Low (with 250 mM KCl) buffer and TCS buffer (no KCl) (**Table 2**).

DNA and octamer were mixed in RB High buffer at desired ratios (0.5:1, 1:1, 1.5:1). Each 20 µL reaction mixture was transferred to a 10 kDa MWCO pre-wetted dialysis button (Slide-A-Lyzer, Thermo Fisher), which was then placed in 400 mL of RB High buffer on a magnetic stirrer. A gradient dialysis was then performed using a dual-head peristaltic pump (Gilson MiniPuls 3) setup to gradually add 2 L of RB Low to the beaker with 400 ml of RB High, while removing the RB High/RB low mixture at the same rate to decrease the KCl concentration to 250 mM maintaining constant volume. The pump speed was set to 6-6.5 rpm, and the dialysis proceeded overnight. On the following day, the dialysis buttons

were transferred to fresh RB Low buffer for 2 hours, and then to TCS buffer for an additional 2 hours to dialyze on a magnetic stirrer at room temperature. The samples were recovered from the membrane and reconstitution efficiency was evaluated using native PAGE (5%, 0.2 x TBE, 150 V, 45 min) and GelRed staining. Once the optimal octamer-to-DNA ratio was identified, the same procedure was scaled up to a total volume of around 60 µL for preparative nucleosome production. The same buffer system, dialysis setup and PAGE conditions were used as described above.

2.8 DNA Processing and End Labeling

2.8.1 Strategy A

Two milligrams of plasmid DNA (25bp linker 2×Widom 601 sequences) were digested with 500 U HindIII-HF and 1100 U EcoRI-HF restriction enzymes in 1× CutSmart buffer. The reaction was incubated at 37 °C overnight. To selectively precipitate the plasmid backbone following digestion, NaCl was added to a final concentration of 500 mM along with 6% PEG 8000. The mixture was incubated on ice for 1 hour, and subsequently centrifuged at 13,000 × g for 20 minutes at 4 °C. The pellet was washed with 700 µL of 70% ethanol, centrifuged again, air-dried, and resuspended in DNA Buffer. The presence of backbone DNA in the resuspended material was verified by 1% agarose gel electrophoresis (1× TAE buffer, 100 V, 50 min) followed by GelRed staining. To prepare biotin-labeled DNA ends, corresponding single-stranded oligonucleotides (**Supplementary Table**) were annealed by mixing each at 100 µM final concentration in 1× Annealing Buffer and adjusting the final volume to 100 µL with nuclease-free water. The mixture was placed in a thermocycler preheated to 95 °C and annealed using a gradient program as described in **Table 6**. Ligation of the annealed double-stranded oligo to the PEG-precipitated DNA fragment was performed by assembling the following reaction: 1 mL of DNA (resuspended in DNA Buffer), 100 µL of the annealed oligonucleotide, 4000 U of T4 DNA ligase, and 122 µL of 10× T4 ligase buffer. The reaction was incubated overnight at 16 °C. The ligase was then heat-inactivated by incubation at 65 °C for 10 minutes. To test ligation efficiency, 500 ng of DNA before and after ligation was digested with BamHI-HF in a reaction containing 2.5 µL of 10× CutSmart buffer, 20 U of BamHI-HF, and nuclease-free water to 25 µL total. After 1 hour of incubation at 37 °C, samples were analyzed by 1.2% agarose gel electrophoresis in 1× TBE buffer stained with GelRed.

2.8.2 Strategy B

For an alternative labeling strategy, 2 mg of plasmid DNA (30bp linker 2× Widom) was digested overnight at 37 °C using 2000 U of EcoRI-HF in 1× CutSmart buffer. Complete digestion was verified on a 1% agarose gel (1× TAE buffer, 100 V, 50 min) stained with GelRed. Following digestion, 100 U of calf intestinal phosphatase (QuickCIP, NEB) were added and the reaction was incubated at 37 °C for 1.5 hours to dephosphorylate DNA ends. To confirm successful dephosphorylation, a ligation test was performed: 50 ng of DNA (before and after CIP treatment) was combined with 2 µL of 10× T4 Ligase Buffer, 2000 U of T4 DNA ligase, and water to a final volume of 20 µL. The ligation reaction was incubated at 16 °C for 10 minutes. Afterwards, 1 µL of the reaction was used to transform 25 µL of competent *E. coli* NEB 5-alpha cells via heat shock. Cells were diluted 10-fold in LB medium and incubated for 30 minutes at 37 °C with shaking. The transformed bacteria were plated on LB agar containing ampicillin and incubated overnight at 37 °C. Colony counts were compared to assess ligation efficiency. Enzymes were heat-inactivated at 80 °C for 5 minutes and cooled to room temperature. HindIII-HF (600 U) was added and the mixture was incubated overnight at 37 °C. Backbone DNA was precipitated by adding NaCl (500 mM final) and 6% PEG 8000 as described above. Biotinylated oligonucleotides were annealed as previously described (final DNA concentration 100 µM in 100 µL), and the resulting duplex was ligated to the PEG-precipitated DNA. The ligation reaction contained 300 µL of DNA fragment, 100 µL of annealed oligonucleotide, 45 µL of 10× T4 Ligase Buffer, and 4000 U of T4 DNA ligase. It was incubated at 16 °C overnight. Ligase was then heat-inactivated at 65 °C for 20 minutes and allowed to cool to room temperature. For ligation verification, a test with cut with SmaI was performed. The digested products were analyzed by 1.2% agarose gel electrophoresis in 1× TBE buffer as described above. For desalting and purification, DNA was precipitated by adding NaCl (500 mM) and two volumes of 96% ethanol. After incubating on ice for 30 minutes, samples were centrifuged at 20,000 × g for 20 minutes at 4 °C, washed with 70% ethanol, and centrifuged again. The pellet was resuspended in 240 µL of DNA Buffer. To perform size-selective precipitation, NaCl (500 mM final) and 5% PEG 8000 were added. The mixture was incubated on ice for 2 hours and centrifuged at 13,000 × g for 20 minutes at 4 °C. The pellet was resuspended in 800 µL of DNA Buffer, and the supernatant was further precipitated by adding 0.7× volume of isopropanol. After centrifugation (13,000 × g, 20 min, 4 °C), the pellet was

washed with 70% ethanol, centrifuged again, air-dried, and resuspended in DNA Buffer. Samples of input DNA, pellet, and supernatant fractions were analyzed by 1.2% agarose gel electrophoresis (1× TAE) stained with GelRed. After unsuccessful attempts on size-selective PEG precipitation, initial trials of anion-exchange chromatography separation were performed as described later in section **2.9**.

2.8.3 Strategy C

Plasmid DNA (15bp linker 2×Widom 601) was digested with SmaI-HF in a reaction composed of 1 mg DNA, 1× CutSmart buffer, and 60 µL of SmaI-HF. The mixture was incubated at 37 °C overnight. Complete digestion was verified by agarose gel electrophoresis on a 1% gel prepared with 1× TAE buffer. Following digestion, the DNA was dephosphorylated by adding 30 U of CIP and incubating the mixture for 2 hours at 37 °C. To assess the efficiency of dephosphorylation, a ligation test was performed as described in **2.8.2**. Enzyme activity was then inactivated by heating the sample at 80 °C for 5 minutes and allowing it to cool to room temperature. Subsequently, 800 U of HindIII-HF were added, and the sample was incubated overnight at 37 °C. To desalt and recover the DNA, sodium acetate was added to a final concentration of 0.3 M along with two volumes of 96% ethanol. The sample was incubated at –20 °C for 30 minutes and centrifuged at 20,000 × g for 20 minutes at 4 °C. The pellet was washed with 70% ethanol, centrifuged again, air-dried, and resuspended in DNA Buffer. DNA was further purified by anion-exchange chromatography, as described in section **2.9**. The concentration of DNA in the eluted fractions was measured using NanoDrop, and the identity of fraction was verified on a 1% agarose gel (TAE). Target fractions were pooled and precipitated with sodium acetate and ethanol.

Single-stranded oligonucleotides (**Supplementary Table**) were annealed following the same procedure described earlier, at a final DNA concentration of 100 µM. For the ligation, 100 ng of isolated DNA was mixed with varying amounts of annealed double-stranded oligonucleotides as shown in **Table 7**. The reaction was incubated at room temperature for 20 minutes. Ligase inactivation was performed by heating the sample at 70 °C for 5 minutes.

To verify biotinylation of the ligated DNA, a bead depletion test was conducted using magnetic streptavidin-coated beads (Thermo Fisher). The bead suspension was thoroughly mixed, and 4 µL of resuspended beads were washed three times with BW Buffer (2 mM Tris-HCl, pH 7.5, 1 mM EDTA, 1 mM DTT, 150 mM NaCl). Then, 4 µL of washed beads were incubated with either 10 or 20 µL (half the volume) of the ligation mixture for 1 hour at room temperature with shaking. Beads were separated on a magnetic rack (MagRack 6, Cytiva) for 3 minutes, and the supernatant was removed. Input and supernatant samples were analyzed on a 1.5% agarose gel (1× TBE buffer) to evaluate depletion of the labeled DNA.

Table 7. Different molar ratios used for ligation of biotinylated DNA adaptors.

Ratio (adaptor:fragment)	V total (µL)	m fragment (ng) (356 bp, 66 ng/µL)	V fragment (µL)	m oligo (ng)	V oligo (µL)	V water (µL)	V buffer (µL)	T4 ligase (µL) (2 MU/mL)
3:1	*20*	*100*	*1.5*	*29*	*1.1*	*14.4*	*2*	*1*
5:1	*20*			*48*	*2*	*13.5*	*2*	
7:1	*20*			*67*	*2.7*	*12.8*	*2*	
9:1	*20*			*86*	*3.5*	*12*	*2*	
30:1	*40*	*100*	*1.5*	*287*	*11.5*	*22*	*4*	*1*
60:1	*40*			*573*	*23*	*10.5*	*4*	
90:1	*40*			*860*	*34*	*0*	*4*	

2.8.4 Klenow-based labelling

Two milligrams of plasmid DNA were subjected to a double cleavage by EcoRI-HF and SmaI. The reaction was performed in 1× CutSmart buffer with 300 U of EcoRI-HF, 300 U of HindIII-HF and with the total volume adjusted with water to keep the DNA concentration under 1 µg/µL. The reaction mixture was incubated overnight at 37 °C. Completion of digestion was confirmed by electrophoresis on a 1.2% agarose gel prepared with 1× TAE buffer. The digested DNA was precipitated using sodium acetate (0.3 M final) and two volumes of ethanol, incubated at -20 °C, and centrifuged as described previously. The DNA pellet was washed, air-dried, and resuspended in 2 mL of DNA Buffer. Purification of the digested DNA was conducted by anion-exchange chromatography (more details provided in section **2.9**). DNA concentration in the eluted fractions was measured using NanoDrop. The identity and integrity of the DNA were assessed by 1.2% agarose gel electrophoresis (1× TAE buffer). Peak fractions containing the target DNA were pooled

and precipitated using sodium acetate (0.3 M final concentration) and 0.7× volume of isopropanol. After centrifugation and washing, the purified DNA was resuspended (to concentration ~1 µg/µL) in preparation for labeling.

For end labelling the reaction mixture contained 200 µL of purified DNA, 50 U of Klenow fragment (NEB), 33 µM each of dATP (NEB) and biotin-11-dUTP (Thermo Fisher), 1× NEB2 buffer, and nuclease-free water to a final volume of 300 µL. The mixture was incubated at room temperature for 40 minutes. The reaction was stopped by adding EDTA to a final concentration of 10 mM and heating the sample at 75 °C for 20 minutes. Labeled DNA was then precipitated with sodium acetate and isopropanol and resuspended in 20-25 µL of RB High buffer. The efficiency of biotin incorporation was verified using a bead depletion test: 50 ng of labeled DNA was incubated with 4 µL of magnetic streptavidin beads, and efficiency was assessed by comparing input and supernatant fractions on an agarose gel as described in the previous section.

2.9 Anion-exchange chromatography

Following restriction digestion, DNA cleaved out from the plasmid vector during the processes described in **Strategy B** and **Klenow-based labelling** was precipitated and the DNA pellet was resuspended in 2-4 mL of AE buffer A to ensure no salt content. The target fragment was purified on MonoQ 5/50 GL Column (Cytiva) and AKTA Pure 25 FPLC (Amersham Biosciences) system in buffers based on 1× DNA Buffer. Before use the column was equilibrated with 10 column volumes (CV) of MiliQ water at 1.5 mL/min, then with 10 CV of AE buffer A (1.5 mL/min). A quick gradient to 100 % AE buffer B was run (over 10 CV, 1.5 mL/min) and then the column was transferred back to starting AE buffer A with 10 CV (1.5 mL/min). The whole procedure including elution was performed at room temperature. After equilibration the sample was manually loaded into the system (5mL sample loop), injected onto the column and then washed with 3 CV of AE buffer A. The elution was performed using a gradient of AE buffer B1 or B2, in other words by a gradual increase in NaCl concentration from 0 to 1 or 2 M, respectively. An overview of the methods and gradient segments are summarized in **Table 8**. Along the experiment the flow rate was set to 1 mL/min and the maximal pressure over the column was set to 4 MPa as instructed in the manual by the manufacturer. During the experiment the absorbance (UV_{280nm}, UV_{260nm} in mAU), conductivity (S/m), concentration of AE buffer B (%) were

monitored and plotted against retention volume. The plot was evaluated using Cytiva Unicorn software. Fractions were analyzed via agarose gel electrophoresis (1% agarose, 1× TAE, stained with GelRed).

Table 8. Overview of anion-exchange chromatography methods and their segments.

Employed in:	Stage		Volume (mL)	Elution buffer %	NaCl concentration (M)
Initial attempts in Strategy B	*Equilibration*		*3*	*0*	*0*
	Sample injection		*10*	*0*	*0*
	Column wash		*3*	*0*	*0*
	Elution	*Segment 1*	*15*	*0-70*	*0-1.4*
		Segment 2	*30*	*70-85*	*1.4-1.7*
		Segment 3	*12*	*85-100*	*1.7-2*
	Equilibration		*7*	*0*	*0*
Later attempts in Strategy B, Strategy C, Klenow-based approach	*Equilibration*		*3*	*0*	*0*
	Sample injection		*10*	*0*	*0*
	Column wash		*3*	*0*	*0*
	Elution	*Segment 1*	*15*	*0-65*	*0-0.65*
		Segment 2	*30*	*65-80*	*0.65-0.8*
		Segment 3	*12*	*80-100*	*0.8-1*
	Equilibration		*7*	*0*	*0*

2.10 Cell culture

HEK 293 cells (obtained from colleague Dr. Vlastimil Král) were cultured on 15 cm tissue culture dishes in Dulbecco's Modified Eagle's Medium (DMEM, Sigma-Aldrich) supplemented with 10% fetal bovine serum (FBS, Sigma-Aldrich), 10% Anti-Anti (Thermo Fisher), and GlutaMax (Thermo Fisher, added to 0.5× final concentration due to glutamate already present in the medium) at 37°C in a humidified atmosphere with 5% CO_2 and passaged at ~100% confluency using 0.25% trypsin (in PBS with 0.01% EDTA and phenol red, Thermo Fisher). Cells were harvested by removing the culture medium and washing once with 10 mL of PBS. After discarding the PBS, 4 mL of 0.25% trypsin was added, and the cells were incubated for 5 minutes at 37 °C. Detached cells were resuspended in 11 mL of medium and collected into tubes. Cells were then pelleted by centrifugation at 150 × g for 1 minute at room temperature. The supernatant was removed, and the pellet was washed with 6 mL of ice-cold PBS, followed by another centrifugation at 150 × g for 1 minute at 4 °C. After removing the PBS, the cell pellets were stored at –80 °C until further use.

2.11 Cell Fractionation

Frozen cell pellets were resuspended in 1 mL of PBS and transferred to 1.5 mL tubes. Cells were pelleted by centrifugation at 150 × g for 1 minute at 4 °C. The supernatant was discarded, and the pellets were resuspended in 1.5× pellet volume of ice-cold Fractionation Buffer A (FBA: 20 mM Tris-HCl pH 7.5, 10 mM KCl, 1.5 mM $MgCl_2$, 10% glycerol, 1× protease inhibitor cocktail (Roche)). The suspension was incubated on ice for 15 minutes. Igepal CA-630 was then added to a final concentration of 0.3125 % (v/v), and samples were gently mixed and incubated on ice for an additional 5 minutes. Following incubation, samples were centrifuged at 2,000 × g for 10 minutes at 4 °C. The resulting supernatant (the cytoplasmic fraction) was collected. The nuclear pellet was washed three times with 500 µL of cold FBA, centrifuging each time at 6,000 × g for 10 minutes at 4 °C.

For sonication-based nuclear lysis, nuclear pellets were resuspended in Nuclear Buffer B (NBB: 20 mM Tris-HCl pH 7.5, 150 mM NaCl, 1.5 mM $MgCl_2$, 10% glycerol, 1× protease inhibitor cocktail), using a volume equivalent to the pellet. Samples were sonicated on ice using a probe sonicator (Soniprep 150 MSE) for five 5-second pulses with 30-second intervals between pulses. After sonication, samples were incubated on ice for 20 minutes. Igepal CA-630 was added to a final concentration of 0.2% (v/v), and samples were incubated for 30 minutes at 4 °C with shaking. Lysate was centrifuged at 14,500 × g for 10 minutes at 4 °C. The resulting nuclear supernatant was collected for downstream applications.

For MNase-based nuclear lysis, nuclear pellets were resuspended in MNase Buffer (MNB: 10 mM Tris-HCl pH 7.6, 15 mM NaCl, 60 mM KCl, 0.1% Igepal CA-630, 1× protease inhibitor cocktail, 10 mM sodium butyrate), using a volume equivalent to the original pellet. Micrococcal nuclease (MNase, NEB) was added at 10 U per plate of cells and the reaction was incubated for 2 minutes at 37 °C with shaking at 400 rpm. $CaCl_2$ was then added to a final concentration of 1.5 mM, followed by an additional 6-minute incubation under the same conditions. The reaction was stopped by adding EDTA to a final concentration of 10 mM. Samples were diluted 2 times with ice-cold Nuclear Buffer C (NBC: 30 mM HEPES pH 7.8, 300 mM NaCl, 0.1% Igepal CA-630, 20% glycerol, 0.4 mM EDTA, 1× protease inhibitors, 10 mM sodium butyrate). Samples were rotated at 4 °C for 45 minutes, followed by incubation in a thermomixer at 1,000 rpm for 15 minutes at 4 °C.

Nuclear debris was pelleted by centrifugation at 16,000 × g for 10 minutes at 4 °C. The resulting nuclear supernatant was collected.

2.11.1 Bradford Assay

Protein concentration of cytoplasmic and nuclear supernatants was determined using the Bradford assay (Bradford, 1976). Pre-mixed Bradford solution (Bio-Rad) was diluted 5 times with deionized water. In a 96-well plate, 180 µL of diluted reagent was added to each well. Samples and BSA standards were diluted 200 times and added in 20 µL volumes. Standards were run in duplicates, and samples in triplicates. After incubation at room temperature for ~10 minutes, absorbance was measured using a plate reader (Tecan Infinite 200) and processed using Magellan software. Absorbance values were averaged and plotted against the concentrations of BSA standards. Linear regression in Excel was applied to generate a calibration curve, which was subsequently used to determine the protein concentrations of the samples.

2.11.2 Western Blotting

Protein samples were diluted with PBS to equal final concentrations based on Bradford quantification. SDS-PAGE sample buffer was added to each sample to 1× concentration, and proteins were denatured by heating at 95 °C for 5 minutes. A total of 24 µg of protein per sample was loaded onto pre-cast 4-20% gradient gels. All Blue molecular weight marker (Bio-Rad) was loaded alongside the samples. Gels were run in MOPS running buffer at 150 V for 45 minutes. Proteins were transferred to nitrocellulose membranes using a wet-transfer system (Bio-Rad Trans-Blot Turbo) at 100 V for 1 hour. For transfer, the MOPS running buffer was supplemented with 20% methanol.

Membranes were blocked for 1.5 hours at room temperature using 1× TBS 1% casein blocking solution. Primary antibodies against histone H3 (4499S, Cell Signaling Technology) and alpha-tubulin (3873S, Cell Signaling Technology) were diluted 1:4000 and 1:2000 respectively in TBST containing 5% casein and incubated with the membrane for 4 hours at 4 °C. After primary antibody incubation, membranes were washed three times with TBST for 5 minutes. Secondary antibodies against mouse and rabbit IgG (3873S and 4499S, Azure Biosystems) were diluted 1:10,000 in TBST with 5% casein and incubated for 1.5 hours at 4 °C in the dark. Following incubation, the membranes were washed twice with TBST and once with TBS, each for 5 minutes. Membranes were dried and imaged

(Azure 600, Azure Biosystems) using imaging channels recommended by manufacturer (IR 700 (excitation at 660 nm) and IR 800 (excitation at 785 nm), respectively).

2.12 Pulldown Experiment

To prepare the immobilized bait for affinity purification, streptavidin-coated magnetic beads were used to capture biotinylated dinucleosomes. Beads were first resuspended thoroughly by gentle pipetting, and 10 µL of the suspension was aliquoted into six 1.5 mL LoBind tubes (Eppendorf). The beads were washed three times with 500 µL of BW Buffer. For each wash, the beads were resuspended by gentle pipetting, separated using a magnetic rack, and the supernatant was discarded. Following washing, 4 µg of biotinylated dinucleosomes in 50 µL of BW Buffer were added to the beads. The samples were incubated at room temperature for 20 minutes on a shaker. After incubation, the beads were separated on a magnetic rack and the supernatant was discarded. The beads were then washed three times with 200 µL of BW Buffer. After the final wash, the beads were transferred to new tubes.

Nuclear extracts were prepared as described in section **2.11** and protein concentration was determined by Bradford assay. Prior to incubation with nuclear extracts, beads were washed once with 200 µL of NBB. Nuclear lysates (0.5 mg total protein per sample) were diluted to a final volume of 200 µL in NBB buffer and added to the prepared beads. Samples were incubated for 2 hours at 4 °C on a rotating mixer and separated using a magnetic rack (supernatant collected as a flow-through sample). Beads were washed twice with 200 µL of NBB. Samples were mixed with SDS-PAGE Sample Buffer and heated at 98°C for 10 min. Beads were quickly centrifuged and separated on magnetic rack. Samples were analyzed using SDS-PAGE (4-20% gradient pre-casted mPAGE gel (Merck), MOPS running buffer, 150 V, 45 min, Spectra BR marker (Thermo Fisher), stained with Coomassie G-250 (SimplyBlue SafeStain, Thermo Fisher).

Before submission to mass spectrometry facility similarly prepared material was washed three times with 200 µL of TBS prepared in LCMS-grade water. The microcentrifuge tube was replaced after the first TBS wash.

3 Results

3.1 Cloning a library of linker-defined DNA constructs into a plasmid vector

The objective was to efficiently generate a two-dimensional library of plasmid-embedded DNA constructs containing a defined number of nucleosome-positioning sequences separated by linkers of specified lengths (**Figure 6B**). The architecture of these constructs (**Figure 6A**) is based on tandem repeats of the Widom 601 sequence, a well-characterized nucleosome-positioning element developed by Lowary and Widom. This sequence possesses intrinsic, sequence-encoded high affinity for histone octamers and adopts a favorable geometry for nucleosome formation (Lowary & Widom, 1998). Each Widom 601 element is flanked by DNA linkers of precisely defined lengths, ranging from 15 to 35 bp in 5bp increments. The core of each construct, comprising the nucleosome-positioning sequences and linker segments, is embedded within a high-copy pUC19 plasmid vector carrying ampicillin resistance as a selectable marker, and is flanked by several essential accessory elements that enable manipulation and propagation of repeats. These include external restriction sites RS1 (EcoRI), RS3 (BamHI), RS4 (SmaI), and an internal site RS2 (HindIII). Additionally, two Gibson homology regions are incorporated: an upstream sequence homologous to the vector backbone and a downstream sequence derived from the 5′ end of the Widom 601 sequence. Together, these homology arms ensure correct orientation and efficient recombination during Gibson Assembly, which is discussed in more detail below.

The initial step in the cloning strategy (outlined in **Figure 7A**) involved generation of linker precursors. For example, a 15bp linker precursor consisting of a single Widom 601 unit flanked by a 15bp linker on the 3′ side was extended using inside-out PCR with primers containing complementary 5 bp overhangs. This PCR product was then circularized via a single-fragment Gibson Assembly reaction, yielding a precursor construct with a 20bp linker. Using the same approach, a 35 bp linker precursor was generated from a 30 bp version. PCR amplification and linearization was confirmed by agarose gel electrophoresis, which revealed bands corresponding to the expected size (~2800 bp), rather than the typical multi-band pattern associated with plasmid isoforms (**Figure 7B,D**). The circularized constructs resulting from single-fragment Gibson Assembly were transformed and

subcloned, and plasmid DNA was isolated for sequence verification. Only clones with perfect sequence alignment confirmed by Sanger sequencing were retained and used for further assembly steps.

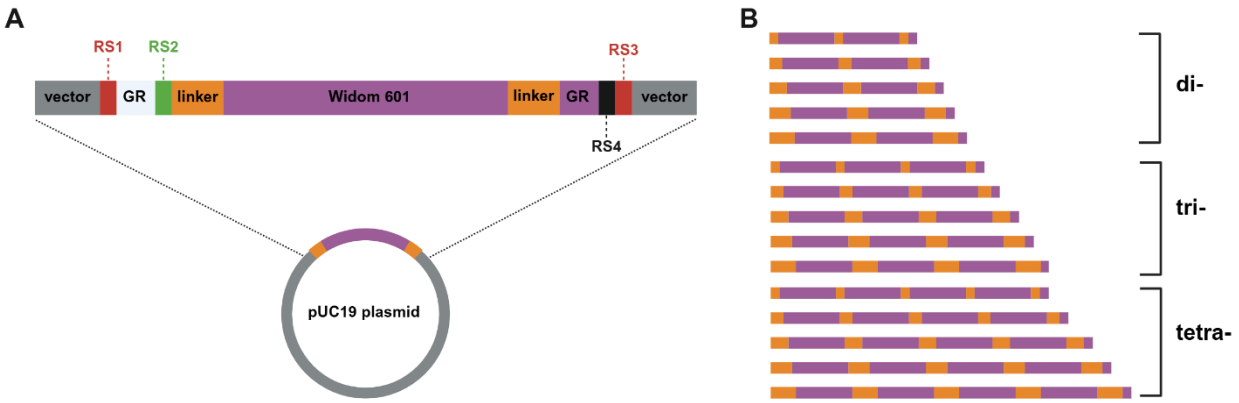

Figure 6. Architecture and key features of DNA constructs. A) All constructs are engineered within high-copy pUC19 plasmid vectors. At the core is always a potent nucleosome-positioning Widom 601 sequence (purple) flanked by variable linker DNA shown in orange. Key features that enable excision and Gibson Assembly-mediated propagation of these Widom repeats include external restriction sites RS1 (EcoRI) and RS3 (BamHI)(red), and internal restriction site RS2 (HindIII, green). Outside of the outermost linker segments are Gibson regions (light blue, purple) that are crucial homology regions for seamless annealing of fragments during propagation. Finally, an external restriction site RS4 (SmaI, black) is used during construct liberation and digestion produces a blunt end to ensure directionality of labeling. **B)** A schematic depiction of the 2D library of DNA constructs to be made. Starting with single Widom constructs described in A) with 15, 20, 25, 30, 35bp linkers the number of repeats is propagated to form constructs for future reconstitution of di-, tri- and tetranucleosomal arrays.

The third step involved another inside-out PCR using primers spanning the junction between the Gibson homology region and the 5′ end of the Widom 601 sequence. The reverse primer in this reaction contained an overhang introducing the HindIII restriction site (RS2). This step served two other purposes: linearization of the plasmid and generating a suitable homology region for repeat multiplication. The success of the PCR reaction was evaluated by agarose gel electrophoresis, which confirmed the presence of a DNA band of the expected size at ~2800 bp (**Figure 7C,E**).

To add the second linker to an RS2-containing precursor, a synthetic double-stranded oligonucleotide was designed. This oligo included the following sequence elements in order: a region homologous to the vector's Gibson sequence, the RS2 restriction site, a linker of defined length, and a segment homologous to the 5′ end of the Widom sequence. This oligonucleotide was inserted into the linearized vector using the Gibson Assembly

reaction. The resulting plasmid contained a single Widom 601 sequence flanked by defined linkers on both sides, along with all necessary elements for subsequent repeat multiplication. Using this strategy, a set of five plasmids was successfully generated, each containing a single Widom 601 sequence flanked by linkers of 15, 20, 25, 30, or 35 base pairs (20 and 35bp linker constructs by myself, others by Dr. Michal Svoboda) (**Figure 8B**). Clones were screened for correct oligonucleotide insertion, and positive clones were validated by Sanger sequencing.

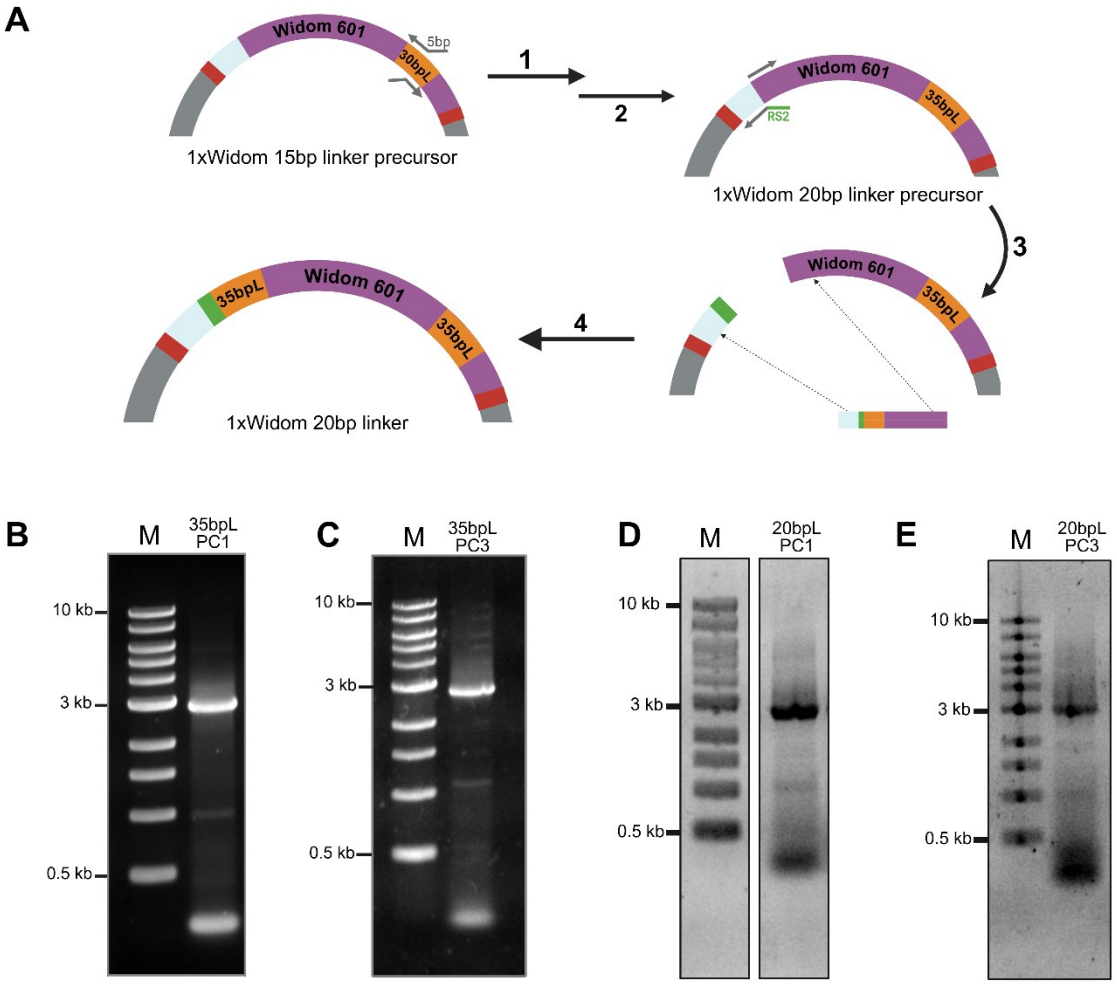

Figure 7. Cloning workflow of a single Widom construct preparation. (A) Starting with a 1×Widom precursor with a 30bp 3' linker, an inside-out polymerase chain reaction (PCR) (1) using primers with 5bp overhangs is performed to expand the linker to 35 bp. The next step is a single fragment Gibson Assembly reaction (2), which closes the vector. Another round of inside-out PCR (3) introduces the RS2 sequence. The linear PCR product is then used for 2-fragment Gibson Assembly (4) to anneal an oligonucleotide, which contains the 5' linker. The resulting product contains a Widom sequence flanked by identical linkers. **(B,D)** The PCR product after step 1 (35bpL PC1, 20bpL PC1) with an expanded linker was analyzed on 0.7% agarose gel showing a band of the desired size at ~3 kb. After the single-fragment Gibson Assembly reaction the sequence integrity was verified by Sanger sequencing. **(C,E)** Similarly, the PCR product after step (35bpL PC3) was analyzed on a 0.7% agarose gel, showing a band at the desired size at ~3 kb. Prior to step 4, the DNA was digested with DpnI and purified.

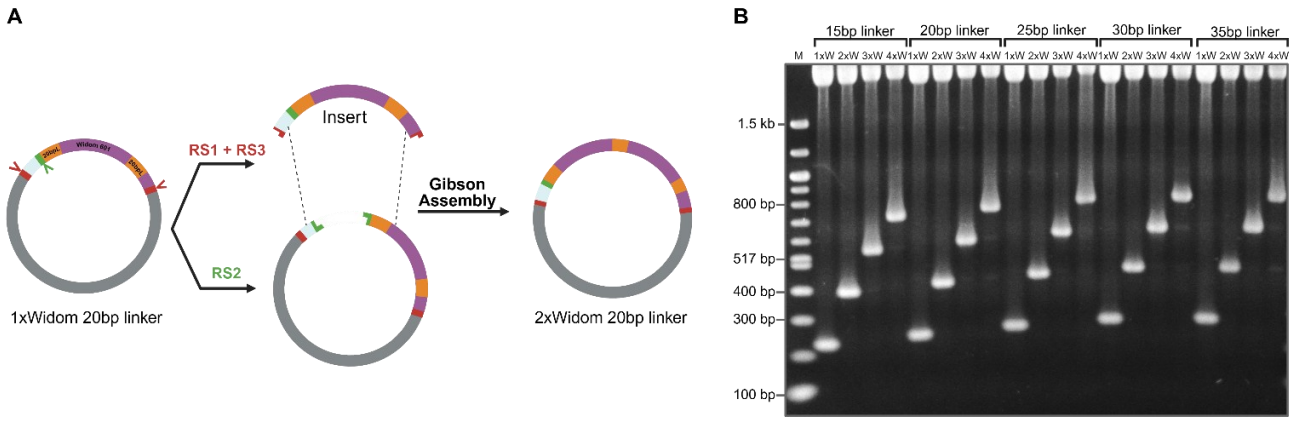

Figure 8. Propagation of Widom repeats. A) To create a 2×Widom construct a 2-fragment Gibson Assembly reaction is used. In this case a 1×Widom plasmid serves as both the insert donor (double cleavage at RS1 and RS3) and the recipient backbone (cleavage at RS2). The generated insert is then separated on 1.5% agarose gel, excised and purified. Correct seamless assembly is verified by Sanger sequencing. **B)** Employing the pipeline described above, a full library (also illustrated in **Figure 6B**) of Widom DNA constructs was prepared. Inserts were cleaved out by restriction enzymes (EcoRI and BamHI) and loaded on 1% agarose gel. Constructs are clustered by linker length (15, 20, 25, 30, 35bp linker) and the number of repeats increases within clusters (1, 2, 3, 4×W).

An approach based on Gibson Assembly reaction was applied using these starting constructs to produce arrays of defined numbers of nucleosome-positioning sequences. A pUC19 plasmid containing a single Widom core sequence was digested at sites RS1 (EcoRI) and RS3 (BamHI), which yields a 1×Widom (5n+10)bp linker insert. The insert is separated by agarose gel electrophoresis and can be used for further propagation once excised and purified from agarose gel (**Figure 8B**). The design of the terminal Gibson homology regions allows for assembling a given number of repeats. For example, if a double Widom construct is desired, the single Widom construct serves as both the insert donor and the recipient backbone. The insert generated by a double digest at RS1 and RS3. The recipient backbone is linearized by restriction digestion at RS2. Insert can then be embedded into the open vector via a Gibson Assembly reaction, utilizing the terminal homologous Gibson regions (**Figure 6A, 9A**). This results in a double Widom plasmid, which can be used for another round of propagation to create a 3 or 4 Widom constructs. In this way, a 2D library of plasmids containing a 1, 2, 3 and 4 Widom repeats was generated (**Figure 8B**) for linkers of 15, 20, 25, 30 and 35 bp. Integrity, precise length of the linkers and the correct number of Widom repeats after the Gibson Assembly reaction was verified by Sanger sequencing in both the forward and reverse directions using M13 sequencing primers, and only plasmids with correct sequence were proceeded with and grown in culture for plasmid isolation.

3.2 Large-scale Plasmid Production

Plasmids need to be produced in large quantities for downstream experiments. For this reason, the plasmids were transformed into competent *E. coli* cells, first grown in starter cultures, which were then used for inoculation and cultivation at the scale of several liters. To obtain the plasmid from culture the approach of alkaline lysis was chosen. This method exploits the general structural differences between plasmid and chromosomal DNAs specifically under alkaline conditions. In the first steps bacterial cells are lysed using a solution containing NaOH and SDS. The high pH denatures both plasmid and genomic DNA, but only plasmid DNA can be renatured, as it is smaller and covalently closed. Genomic DNA remains denatured upon neutralization is precipitated together with cell debris. Plasmid DNA was size-selectively precipitated with polyethylene glycol (PEG), extracted and purified by phenol-chloroform extraction. The presence of the target plasmid along the

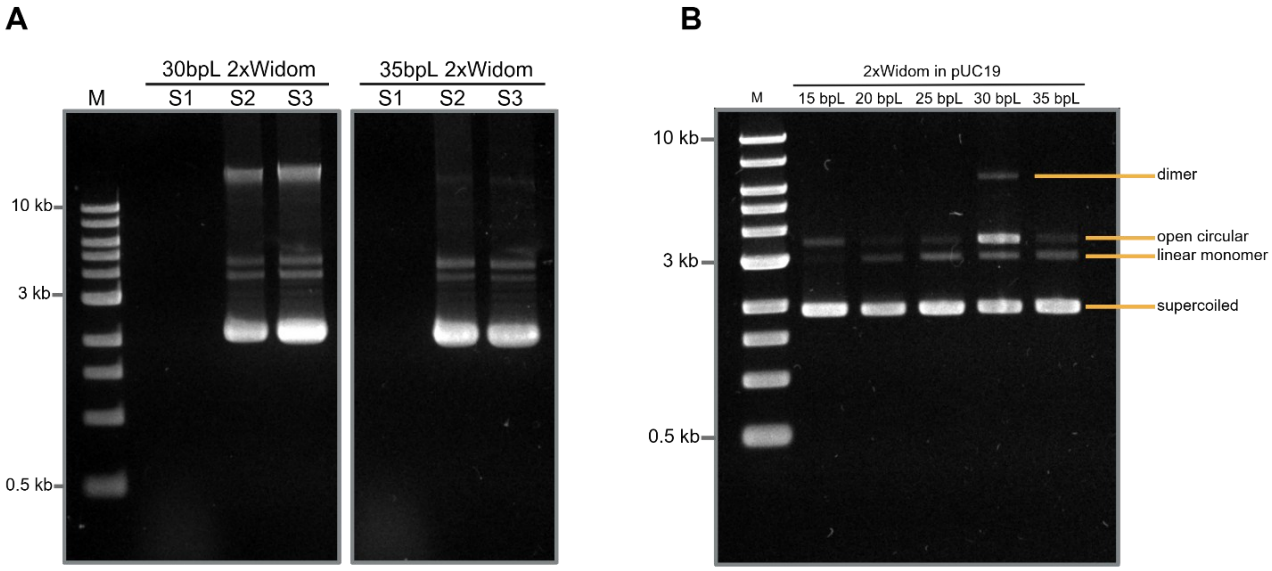

Figure 9. Large-scale plasmid production procedure. A) The presence of target plasmid DNA (2×Widom with 30 and 35bp linkers shown) was verified during isolation at several stages. Samples were analyzed on 1% agarose gel. Sample 1 (S1) represents the supernatant after PEG precipitation and centrifugation, hence no DNA in this sample. Sample 2 (S2) is the resuspended pellet after PEG precipitation showing a pattern of plasmid isoforms. Sample 3 (S3) is supernatant after resuspended pellet was cleared by centrifugation showing no loss of material. Samples were run on the same gel, lanes were rearranged for clarity **B)** The whole set of 2×Widom plasmids with variable linkers (15, 20, 25, 30, 35 bpL) was produced in large scale (tens of milligrams). Samples of the resulting plasmid DNA were analyzed on 1% agarose gel showing that most of the plasmid is enriched for the supercoiled covalently closed form which migrates faster the linear or nicked (open circular) isoforms.

isolation process was monitored by agarose gel electrophoresis (**Figure 9A**). With this approach the whole linker-defined set of 2× Widom plasmids was obtained (**Figure 9B, Figure Figure 10**). The yield of this procedure was assessed by measuring absorbance

at 260 nm. Each plasmid prep was spectrophotometrically assessed for purity represented by ratios A_{260}/A_{280} (indicates protein contamination, ideal values >1,8) and A_{260}/A_{230} (indicates contamination from salts and organic compounds, ideal values >2,0) consistently showing values indicative of highly pure plasmid DNA. The procedure was reproducibly showing average yields of around 11 mg of plasmid DNA per 1 L of culture (

Table 9. Yield and purity of DNA from large-scale.

Construct ID	Yield (g biomass/L culture)	Yield (mg plasmid/L culture)	A260/A280	A260/A230
Table 9. Yield and purity of DNA from large-scale plasmid production				
Construct ID	Yield (g biomass/L culture)	Yield (mg plasmid/L culture)	A_{260}/A_{280}	A_{260}/A_{230}
2×Widom 20bp linker	*13,3*	*11,5*	*1,90*	*2,32*
2×Widom 25bp linker	*13,3*	*11,6*	*1,91*	*2,31*
2×Widom 30bp linker	*12,9*	*10,1*	*1,89*	*2,32*
2×Widom 35bp linker	*13,0*	*15,5*	*1,98*	*2,31*
2×Widom 40bp linker	*11,1*	*6,7*	*1,90*	*2,34*
2×Widom 45bp linker	*13,3*	*11,6*	*1,90*	*2,32*
2×Widom 50bp linker	*13,5*	*14,6*	*1,91*	*2,37*
2×Widom 55bp linker	*12,9*	*10,4*	*1,89*	*2,32*
2×Widom 35bp linker	*13,0*	*15,5*	*1,98*	*2,31*

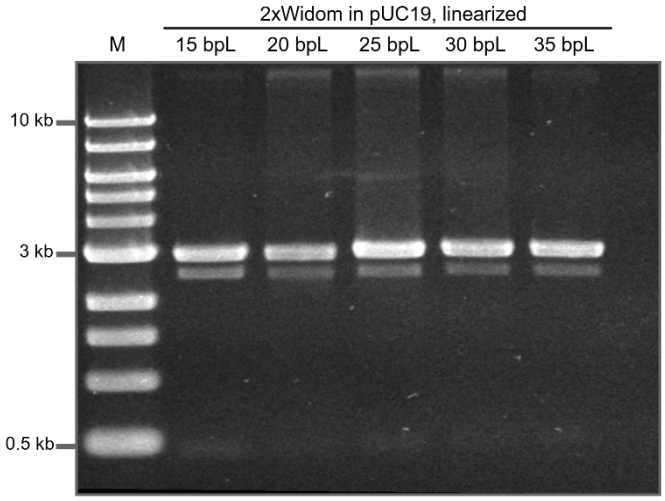

Figure 10. Large-scale plasmid production. Whole set of final plasmid DNAs (full 2×Widom plasmid with variable linkers) as in **Figure 9** was linearized with HindIII and analyzed on 1.2% agarose gel to verify whether all populations represent the same plasmid DNA present in different isoforms. The distinct bands at ~3 kb confirm the plasmid identity.

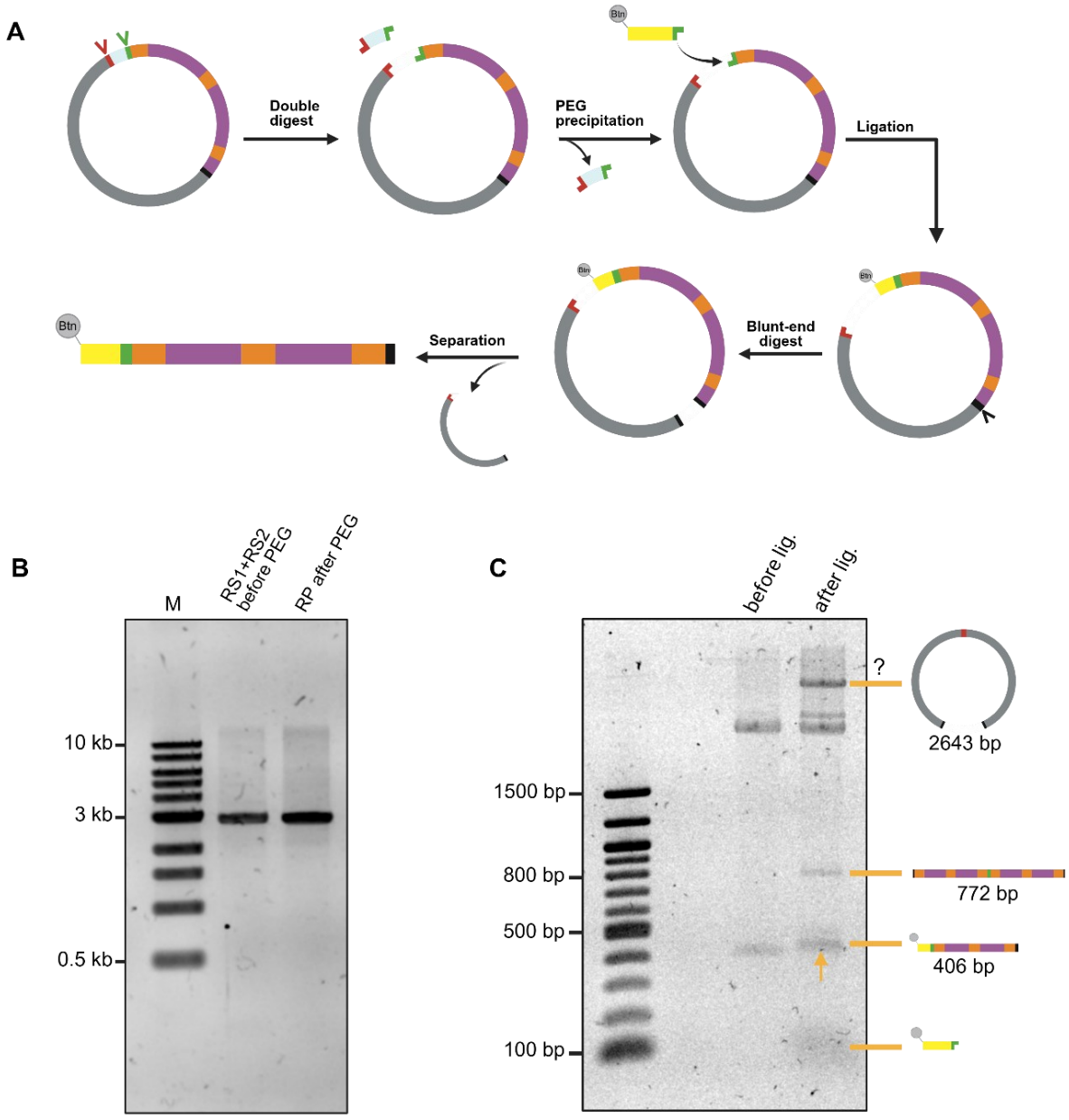

Figure 11. Initial strategy of Widom DNA construct isolation and labeling (Strategy A, 25bp linker 2×Widom plasmid). A) The process starts by a double cleavage at RS1 (EcoRI) and RS2 (HindIII) producing a 26bp fragment (light blue). To prevent unwanted ligation into this small fragment, size-selective PEG precipitation is performed as a separation step. Next, a biotinylated DNA adapter (shown in yellow) with a HindIII overhang is ligated. The resulting DNA is cleaved at RS4 to remove the plasmid backbone, which then must be separated. **B)** DNA after cleavage at RS1 and RS2 before PEG precipitation and the resuspended pellet after PEG precipitation were analyzed on 1% agarose gel. The single distinct band at ~3 kb verifies the presence of the cleaved DNA after precipitation. It however does not confirm separation of the 26bp fragment. **C)** Ligation outcome (after BamHI treatment) analyzed on 1.2% agarose gel. Samples before and after ligation were run. The post-ligation sample contains a shifted band between 400 and 500 bp (indicated by orange arrow) suggesting ligation of the adapter. Additional byproducts include the head-to-head construct ligated via HindIII overhangs (~800 bp) and a high-Mw byproduct potentially being the backbone ligated via EcoRI overhangs.

3.3 Nucleosomal DNA Separation and Labeling

It is important to note that, up to this point, all manipulation with DNA constructs intended for nucleosome reconstitution was carried out with the constructs embedded within a plasmid vector. For downstream applications, the insert must be excised by a double restriction digest and, ideally, purified away from the plasmid backbone. Residual backbone DNA could interfere with later steps such as labelling or nucleosome reconstitution. Biotinylation was chosen as the labeling strategy, as it is widely used for immobilization in pull-down assays. Single-end biotinylation enables specific, oriented and stable attachment of reconstituted nucleosomal arrays to streptavidin-coated magnetic beads.

The original strategy was to use biotinylated DNA adapter oligonucleotides with a single-stranded overhang compatible with a HindIII (RS2) overhang in the recipient vector. These oligonucleotides were first annealed to form double-stranded adapters, which were then used for ligation with the vector using T4 DNA ligase.

The labeling workflow (Strategy A, **Figure 11A**) began with a double restriction digest at RS1 and RS2, which excised a small 26 bp fragment. This short fragment was removed by selective PEG precipitation. The longer plasmid backbone-containing fragment was retained in the pellet (**Figure 11B**) and subsequently ligated with the biotinylated adapter. To assess ligation efficiency, an analytical restriction digestion was performed at RS3 (BamHI) to generate a shorter DNA fragment for improved resolution during agarose gel electrophoresis. Because the inserted adapter was only ~20 bp long, the shift between ligated and unligated products would not be detectable on the full-length backbone. However, by digesting closer to the ligation site, the resulting fragment was short enough for the ~20 bp shift to become somewhat detectable (**Figure 11C**). Unexpectedly, despite using a 6× molar excess of the adapter oligonucleotide relative to the vector fragment, the ligation reaction produced a notable byproduct: two recipient fragments ligated head-to-head via their HindIII overhangs, forming an ~800 bp product (**Figure 11C**). Another byproduct was possibly a large head-to-head dimer of plasmid backbone ligated via RS1 (EcoRI) overhangs (**Figure 11C**).

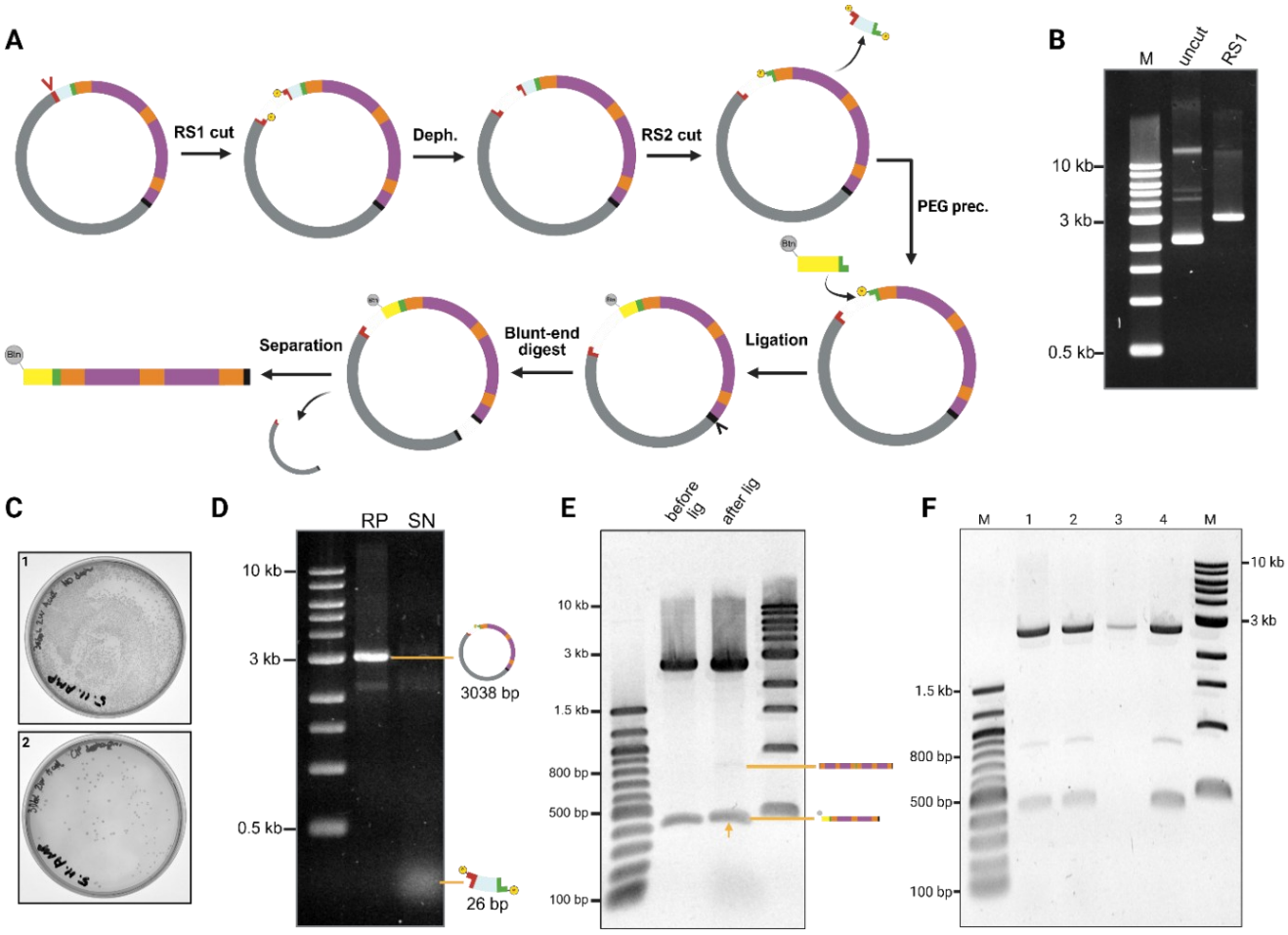

Figure 12. Revised strategy for Widom DNA construct processing and labeling (Strategy B, example with 30bp linker 2×Widom plasmid) A) The procedure begins with a cleavage at RS1 followed by enzymatic dephosphorylation of DNA ends to prevent religation. The DNA is then further cleaved at RS2, and the 26bp fragment (light blue) is separated by size-selective PEG precipitation. Following the separation, biotinylated DNA adapter (yellow) is ligated, the DNA is cleaved at RS4 and separated. **B)** 1% agarose gel confirmation of plasmid digestion by EcoRI, showing a single band of linearized DNA at ~3 kb. **C)** Confirmation of efficient enzymatic (CIP) dephosphorylation by performing a ligation test with samples before (**1**) and after (**2**) dephosphorylation. After short incubation competent *E. coli* bacteria were transformed with ligation mixtures and plated on LB agar plates with ampicillin. Bacteria transformed with dephosphorylated DNA (**2**) formed significantly less colonies indicating that less 5 ‘ phosphate groups were available for ligation. **D)** 1% agarose gel comparing the resuspended DNA pellet (RP) and supernatant (SN) after size-selective PEG precipitation confirming the presence of 3kb DNA fragment in the pellet and hinting that the 26bp fragment remained in solution. **E)** The outcome of ligation analyzed on a 1.2% agarose gel. Samples before and after ligation (after SmaI treatment) were run. A noticeable shift of the bottom band (indicated by orange arrow) confirms ligation. Although the high-Mw ligation byproduct was eliminated by dephosphorylation the head-to-head ligated Widom-containing byproduct (~800 bp) was still present. **F)** 1.2% agarose gel with samples from the process of size-selective precipitation by PEG 8000 (5%) and 500mM NaCl (after SmaI cleavage). Lane **1** is input DNA after SmaI treatment showing 3 populations: biotinylated 2×Widom construct (~500 bp), 4×Widom ligation byproduct (~800 bp) and the plasmid backbone (~2600 bp). Lane **2** is supernatant after precipitation, containing all three populations as well. Lane **3** is resuspended pellet after precipitation showing that only a small portion of the plasmid backbone was separated. Lane **4** is DNA recovered after resuspension was re-precipitated with ethanol and NaCl.

To improve the overall efficiency of the DNA preparation pipeline and to prevent undesired religation at RS1, the order of enzymatic steps was revised. In the modified strategy (Strategy B, **Figure 12A**), the process began with restriction digestion at RS1 (**Figure 12B**), followed by dephosphorylation of 5′ DNA ends using calf intestinal alkaline phosphatase (CIP) (**Figure 12C**). This was intended to reduce nonspecific religation during subsequent steps. The dephosphorylated DNA was then digested at RS2, generating the same 26 bp fragment as before, which was again removed by selective PEG precipitation and confirmed by agarose gel electrophoresis (**Figure 12D**). Even though the large ligation byproduct consisting of two backbones joint together via RS1 was eliminated by prior dephosphorylation, the dimer of Widom constructs joint via RS2 was still visible on agarose gel (**Figure 12E,F**). To isolate the target ligation product from both plasmid backbone and byproducts, a second round of PEG precipitation was attempted. Unfortunately, this

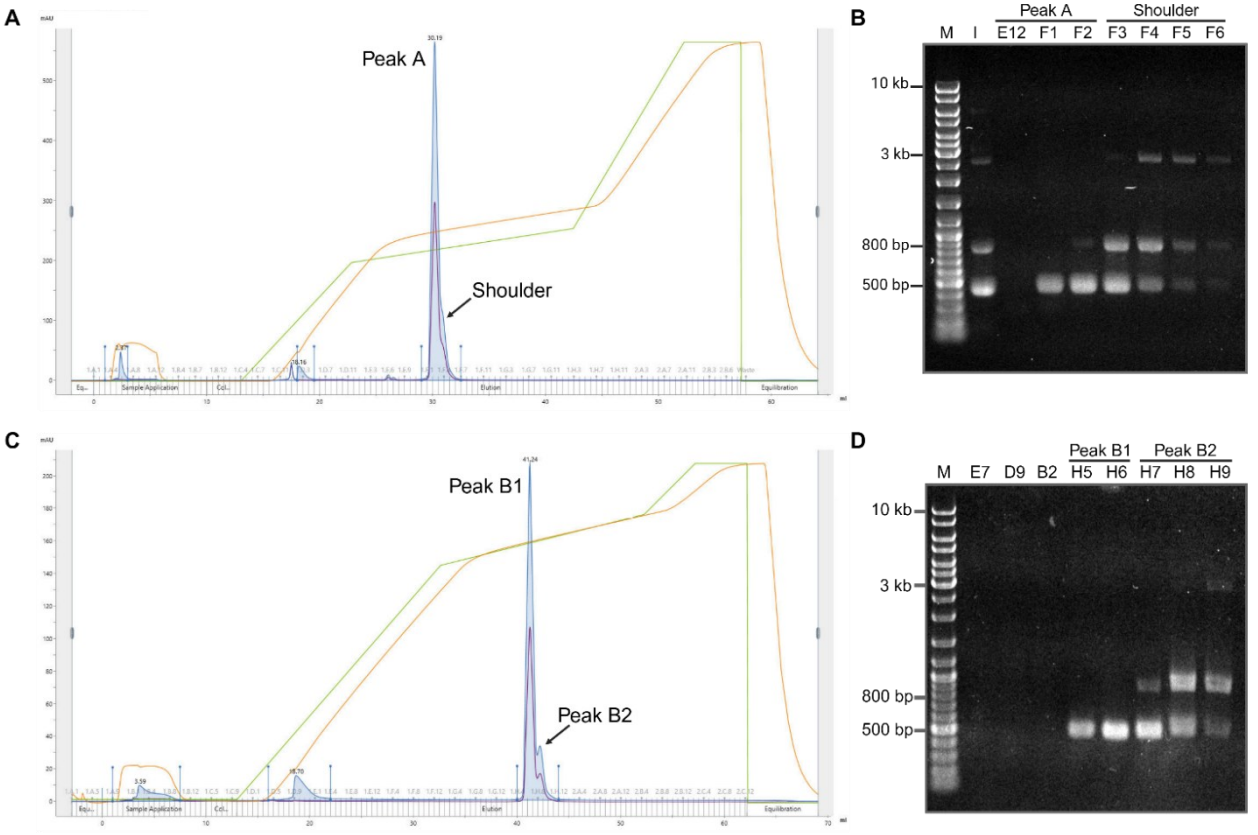

Figure 13. Initial attempts of DNA separation by anion-exchange chromatography (MonoQ 5/50 GL column) in the last step of Strategy B (Figure 10). A) Profile of gradient elution (0→2 M NaCl) showing a single peak with a slight shoulder (green – concentration of NaCl, orange – conductivity, blue – UV_{260} absorbance, purple – UV_{280} absorbance) **B)** Agarose gel electrophoresis of input DNA (I) and fractions corresponding to peak A and its shoulder from **A**. **C)** Profile of gradient elution from the second run (0→1 M NaCl) showing a split peak. **D)** Agarose gel electrophoresis of fractions corresponding to the peaks B1 and B2 from **C.**

step failed to effectively remove the backbone, as most of it remained soluble under the selected PEG conditions (5% PEG, 500 mM NaCl) (**Figure 12F**).

As an alternative approach, anion-exchange chromatography was explored. At first, multiple attempts with a 0→2 M NaCl elution gradient failed to resolve the ~350bp size difference between the desired fragment and the ligation byproduct. The chromatogram showed a single peak with a slight shoulder (**Figure 13A**), but agarose gel electrophoresis of respective fractions revealed that the larger fragments eluted later than the shorter target fragment (**Figure 13B**). Fractions from the peak were pooled, ethanol-precipitated and run again, but using a different elution gradient (0→1 M NaCl). The second round of chromatography produced a split peak (**Figure 13C**), and fractions on agarose gel showed promising separation of the target biotinylated DNA: the higher-Mw backbone was separated efficiently, and some fractions appeared to contain primarily the biotinylated target fragment (**Figure 13D**).

To simplify the workflow, minimize loss of labeled material from repeated precipitation steps, and avoid the accessory RS1 digestion, the pipeline was revised again. This new strategy (Strategy C, **Figure 15A**) began with a blunt-end restriction digest at RS4 (SmaI), followed by CIP-mediated dephosphorylation. The open, dephosphorylated plasmid was then digested at RS2 (HindIII), yielding the target insert and the plasmid backbone (**Figure 15E**). Since both carry HindIII overhangs, effective separation was essential to prevent undesired adapter ligation into the backbone. Importantly, the size difference between the two DNA fragments was now larger, increasing the potential of separation by anion-exchange chromatography. A shallow salt gradient (0→1 M NaCl) was used, and the NaCl concentration was held constant manually when peaks in 260nm absorbance began to appear. This way the fragments were successfully separated (**Figure 14Figure 15**), desired fractions were pooled, and DNA was recovered by alcohol precipitation.

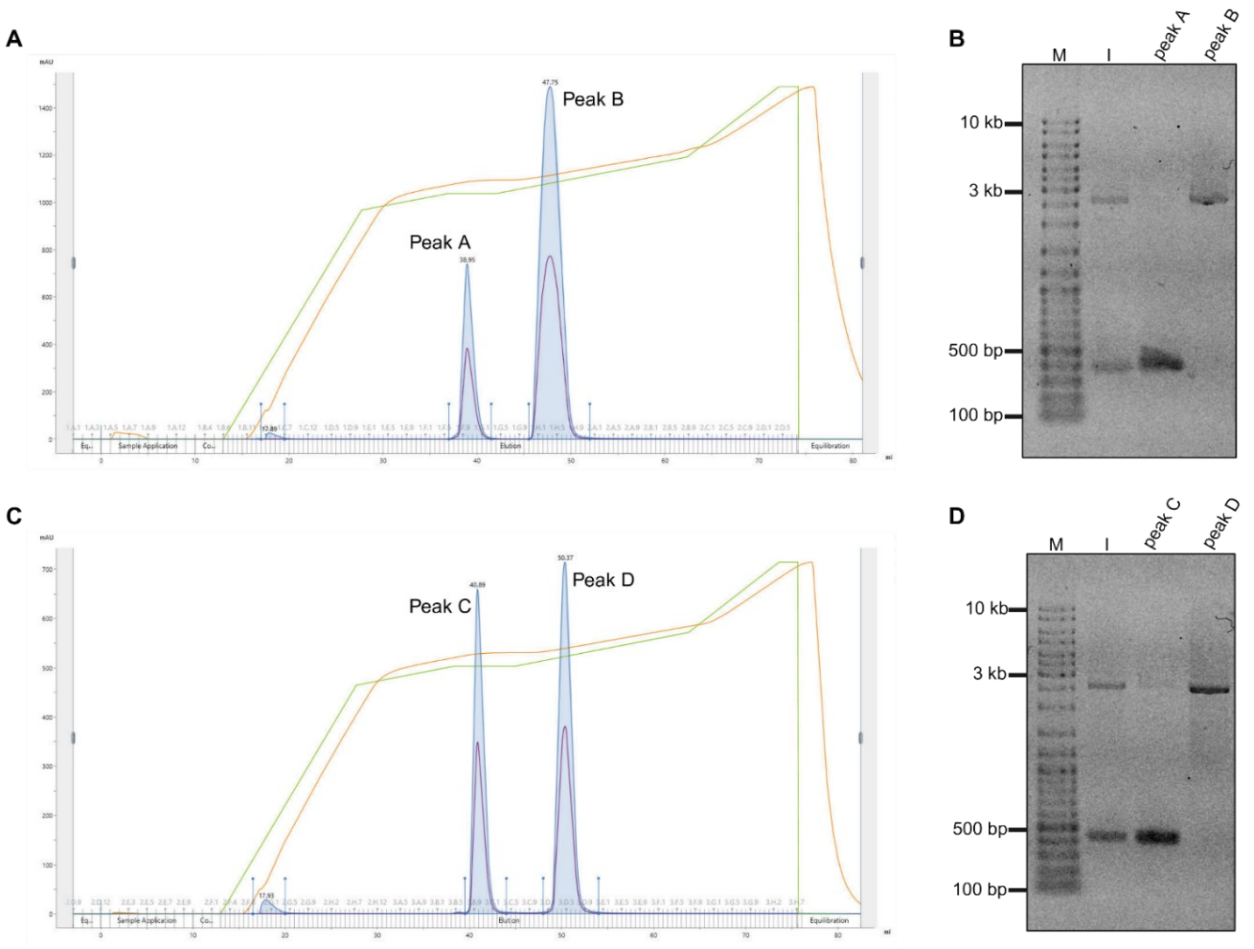

Figure 14. DNA separation by anion-exchange chromatography. A) The profile of a gradient elution (0→1M NaCl) with a manual hold after peak in UV_{260} began to appear (green – concentration of NaCl, orange – conductivity, blue – UV_{260} absorbance, purple – UV_{280} absorbance). 15bp linker 2×Widom construct was separated from plasmid backbone. **B)** Input DNA (I) and fractions corresponding to peaks A and B were analyzed on 1% agarose gel, confirming separation of plasmid backbone from target DNA fragment **C)** The profile of a gradient elution using the same conditions as in **A**. 30bp linker 2×Widom construct was separated from plasmid backbone. **D)** Input DNA (I) and fractions corresponding to peaks C and D were analyzed on 1% agarose gel, confirming separation.

Despite these improvements, subsequent ligation with biotinylated DNA adapters still resulted in noticeable formation of ligation byproducts, even when a significant molar excess of the adapters was used (**Figure 15B,C,D**). At 3:1, 5:1, 7:1 and 9:1 adapter-to-fragment molar ratios, the preferred outcome of ligation was not favored, and the reaction consistently produced the self-reacted 2×Widom byproduct of around 800 bp (**Figure 15C**). Samples of the ligation mixture was incubated with streptavidin-coated beads, and input versus supernatant were analyzed on an agarose gel to assess the efficiency of biotinylation. The same was done for unlabeled DNA to rule out non-specific binding to beads (**Figure 15B**). This revealed that the shifted band above the original ~400bp band

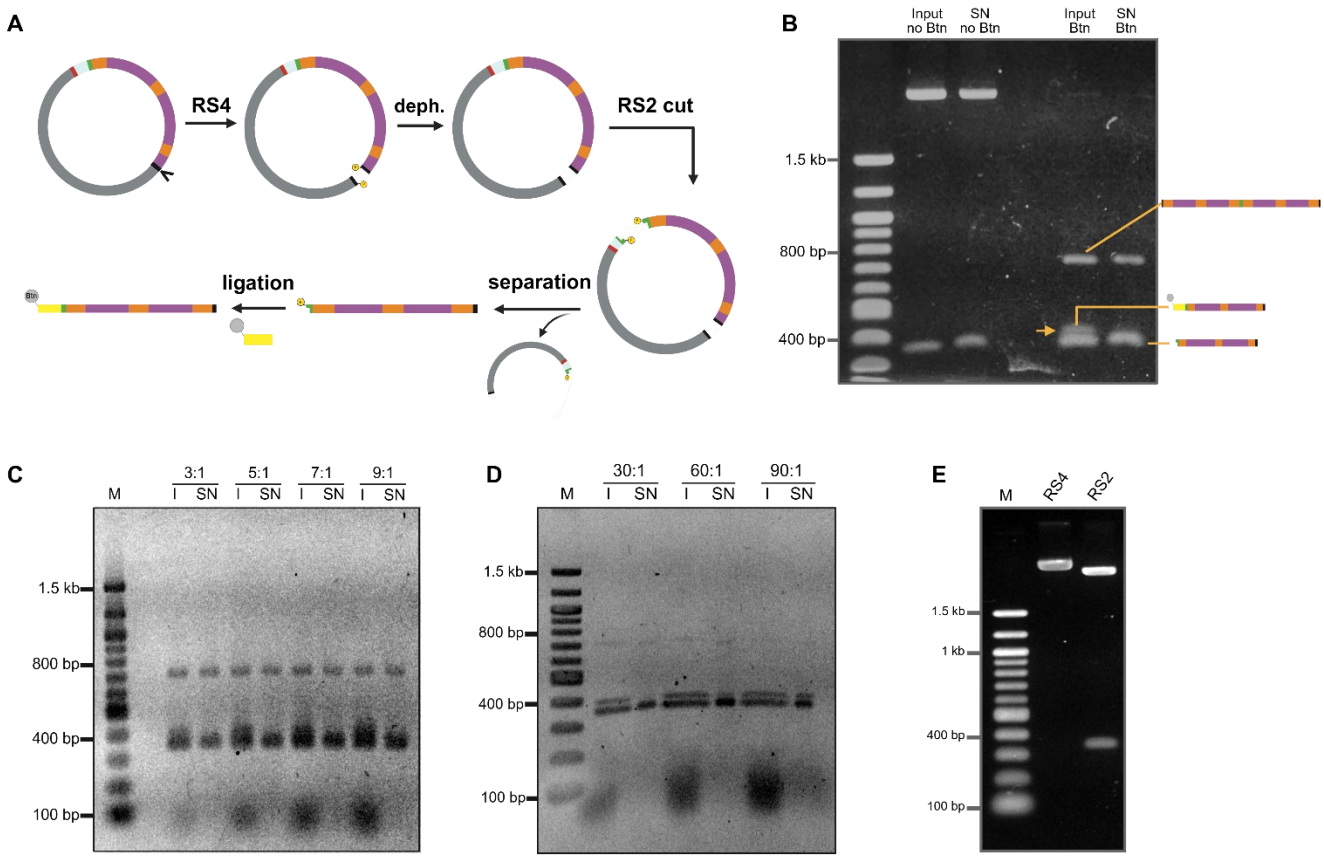

Figure 15. Alternative pipeline (Strategy C) for Widom DNA constructs processing and labelling (Example with 15bp linker 2×Widom plasmid) A) The process begins with a blunt cut at RS4 by SmaI followed by CIP dephosphorylation of DNA ends. Linear DNA is then cut at RS2 by HindIII and the plasmid backbone separated by AE chromatography. After the separation, the biotinylated DNA adapter (yellow) is ligated to the Widom DNA construct. **B)** 1.5% agarose gel with samples of unlabeled DNA (no Btn) and DNA after ligation of biotinylated adapters (Btn) comparing input (I) and supernatant after incubation with magnetic streptavidin-coated beads (SN). The unlabeled DNA did not bind to the beads non-specifically. Ligation was incomplete at 3:1 molar ratio of adapter to construct, and produced the head-to-head dimer byproduct (band at ~800 bp). A fraction of the DNA was labeled with biotin as the shifted band (indicated by orange arrow) was depleted from solution upon incubation with beads. **C) and D)** Similar analysis of ligation outcome as described above in **B**. after ligation at 3:1, 5:1, 7:1, 9:1, 30:1, 60:1, 90:1 adaptor-to-construct molar ratios. Ligation was incomplete at these ratios, and the dimer byproduct was not eliminated. At 60:1 and 90:1 ratios the unreacted adaptor (density at the bottom of the gel) preferentially saturated the beads during immobilization. **E)** 1% agarose gel with samples of plasmid DNA digested by SmaI (RS4) and subsequently by HindIII (RS2) showing that the target was fully cleaved out (band at ~400 bp).

may represent the correctly biotinylated fragment as it is efficiently depleted from the solution after magnetic separation by beads (**Figure 15B,C,D**). However, some of the target fragment remained unreacted, even though lots of the biotinylated adapter were available and depleted upon incubation with beads (**Figure 15B,C,D**). The same analysis was performed applying even higher molar excesses (30:1, 60:1, 90:1). This led to a relative reduction of the unwanted 800bp population, but much of the target fragment remained unlabeled. Additionally, at these higher molar excesses, namely 60:1 and 90:1, during

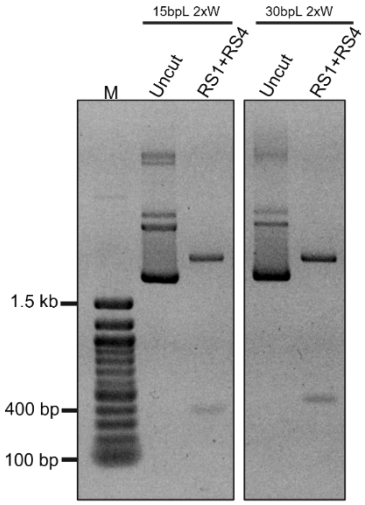

Figure 16. Cleavage of target 2×Widom constructs prior to anion-exchange chromatography. 1.2% agarose gel with samples of plasmid DNA (15bp linker 2×Widom, 30bp linker 2×Widom) before and after double-cut at RS1 (EcoRI) and RS4 (SmaI).

immobilization test the unreacted adapter (density at the bottom of gels) outcompeted the labeled fragment and was preferentially depleted from solution (**Figure 15D**).

These limitations led to the adoption of a more straightforward strategy with a different mechanism. It employed the Klenow fragment of *E. coli* DNA polymerase I, which lacks exonuclease activity and is commonly used for blunting 5′ DNA overhangs. The principle of this approach lies in enzymatic fill-in of a cohesive end using a nucleotide mix, where one of the deoxyribonucleotides carries a biotin modification (**Figure 17A**). This reaction does not only blunt the overhang, but simultaneously introduces a terminal biotin label suitable for immobilization. To implement this strategy, the plasmid was digested with EcoRI (RS1) and SmaI (RS4), generating two fragments. Successful cleavage was confirmed by agarose gel electrophoresis, showing distinct bands at ~400 bp and ~2600 bp

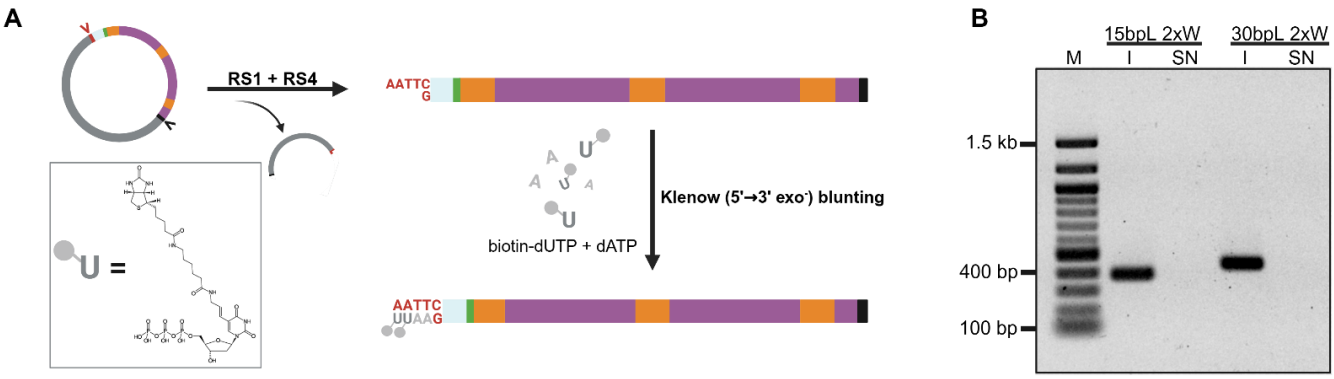

Figure 17. Klenow fragment-based biotinylation strategy. A) The plasmid DNA is first double-cleaved at RS1 and RS4, and the long plasmid backbone is separated by anion-exchange chromatography. 5' overhang generated by EcoRI (RS1) is filled-in using the Klenow fragment of DNA Polymerase I supplied with dATP and biotin-11-dUTP. **B)** Klenow-based biotinylation was verified via incubation of DNA with streptavidin-coated beads. Input (I) and supernatant after immobilization and magnetic separation (SN) were analyzed on 1% agarose gel. Successful labeling is manifested by total DNA depletion from solution after incubation with beads.

(**Figure 16**). The two fragments were then separated using the previously optimized anion-exchange chromatography protocol. Efficient separation was achieved by carefully holding the NaCl concentration in the elution buffer at approximately 0.7 M, coinciding with the onset of UV absorbance peaks. Fractions containing the desired insert were pooled and purified via isopropanol precipitation in the presence of sodium acetate. To evaluate biotin incorporation, a small aliquot of the purified DNA was incubated with streptavidin-coated magnetic beads. Input and supernatant samples were analyzed by agarose gel electrophoresis. The complete depletion of DNA from the supernatant indicated highly efficient labeling (**Figure 17B**).

3.4 Histone Octamer Refolding

In addition to the biotin-labeled DNA containing the nucleosome-positioning sequence, the second essential component for nucleosome reconstitution is a native histone octamer. Unmodified histone proteins were mixed in equimolar ratios under strongly denaturing conditions to ensure complete unfolding and disaggregation of individual subunits. This mixture was then subjected to dialysis against a non-denaturing refolding buffer for octamer assembly. Following refolding, the sample was subjected to size-exclusion chromatography to isolate fully assembled histone octamers. The octameric complex eluted at approximately 15 ml (**Figure 18A**). Fractions corresponding to this elution volume were analyzed by SDS-PAGE, which confirmed the presence of all four core histones (H2A, H2B, H3, and H4), represented by a distinct band pattern (**Figure 18B**). The middle band commonly appears as one strong band, as it contains both H2A and H2B, which are of similar size. The gel pattern suggests that the broad low-intensity signal in front of the main peak most probably represents aggregates of histone proteins, whereas the smaller peak behind mostly contains assembly intermediates such a H2A/H2B dimers and H3/H4 tetramers.

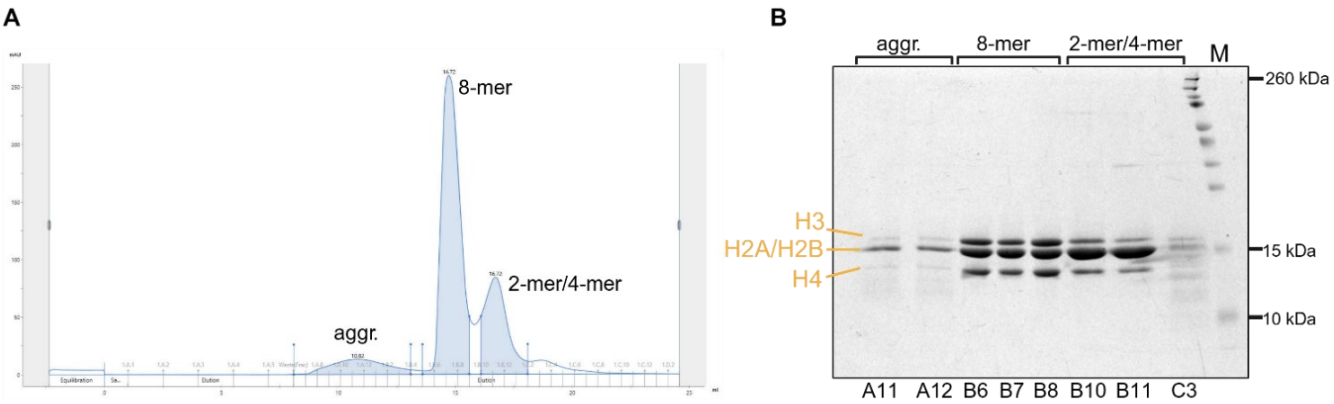

Figure 18. Refolding and purification of recombinant histone octamers. (A) Size-exclusion chromatography (SEC) profile of refolded histone octamers. **(B)** SDS-PAGE analysis of fractions from SEC. Fractions corresponding to the major octamer peak (8-mer) contain equimolar amounts of histone proteins, confirming successful refolding. Smaller represents histone tetramers and dimers (2-mer/4-mer). The earlier eluting broad peak could correspond to aggregated material (aggr.).

3.5 Reconstitution of Dinucleosomal Arrays

To assemble the biotinylated nucleosomal arrays intended for affinity purification experiments, labeled DNA constructs were wrapped around refolded histone octamers. As an initial test, a small-scale reconstitution was performed using the 2×Widom 601 construct with a 15 bp linker. This test used a 1:1 molar ratio of histone octamer to DNA and utilized a stepwise dilution method. Native PAGE analysis of the final assembly mixture showed evidence of partial nucleosome formation, with some DNA appearing in slower-migrating bands, while a significant portion remained unshifted. The gel also revealed multiple intermediate species, likely representing mononucleosomes and partially assembled particles, indicating that the reaction conditions were not yet optimized (**Figure 19A**). To determine the optimal ratio for an efficient dinucleosomes assembly, gradient dialysis was performed as the next step. Small-scale reconstitutions were carried out at 0.5:1, 1:1, and 1.5:1 octamer-to-DNA ratios using 15bp and 30bp linker 2×Widom constructs. Native PAGE analysis (**Figure 19B**) showed that a 0.5:1 ratio resulted in under-saturation of DNA with histones, which was apparent from the presence of multiple species and unbound DNA. In contrast, both the 1:1 and 1.5:1 ratios significantly reduced the amount of free DNA. The 1.5:1 ratio introduced a diffuse smear above the main nucleosome band. Based on these results, the 1:1 ratio was chosen as the condition for large-scale nucleosome reconstitution. Larger-scale reconstitution reactions using this optimized ratio were again performed using gradient dialysis, and the products were again analyzed by native

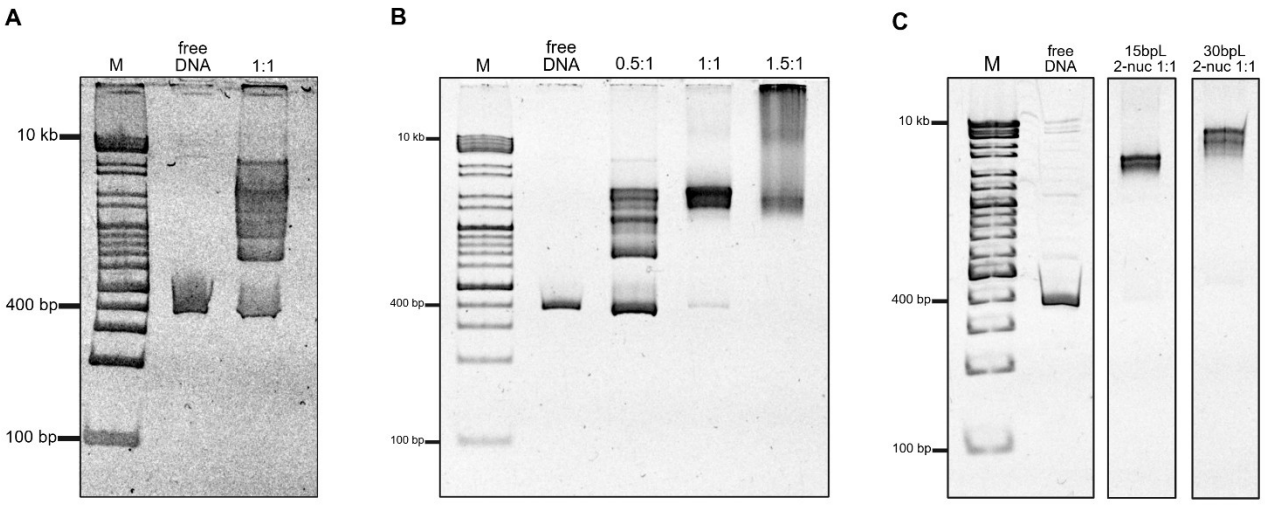

Figure 19. Native PAGE analysis of nucleosome reconstitution. (A) Small-scale reconstitution of 15bp linker di-nucleosomes (15bp linker) at a 1:1 molar ratio of histone octamer to DNA using stepwise dilution, analyzed on 5% native PAGE. The upward shift compared to free DNA indicates partial nucleosome formation. **(B)** Optimization of octamer:DNA ratio in small-scale reconstitutions using gradient dialysis (same DNA construct). Ratios of 0.5:1, 1:1, and 1.5:1 were tested. The 0.5:1 ratio yielded under-saturated DNA with multiple intermediate species, 1:1 produced near-complete shifting of DNA into nucleosomal bands, and at 1.5:1, excess octamers resulted in high-Mw aggregates. **(C)** Large-scale reconstitution by gradient dialysis at a 1:1 ratio for 15 and 30bp linker di-nucleosomes. Both showed upward shifts with minimal free DNA, confirming efficient nucleosome assembly at larger scale.

PAGE. The gel showed clear, upwardly shifted bands consistent with di-nucleosome formation, and only minimal traces of free DNA, confirming the success of the protocol at this larger scale (**Figure 19C**).

To estimate the binding capacity of streptavidin-coated magnetic beads, used downstream for pulldown experiments, a titration experiment was performed. In this setup, the amount of beads was kept constant and increasing amounts of biotinylated di-nucleosomes were added. After incubation, magnetic separation was followed by spectrophotometric analysis of the DNA remaining in the supernatant. Plotting the amount of bound DNA against input DNA produced a hyperbolic curve, indicating specific binding behavior (**Figure 20**), and helped to estimate the binding capacity of beads. However, full saturation was not reached within the tested range, suggesting that either higher input concentrations or adjusted bead quantities should be tested.

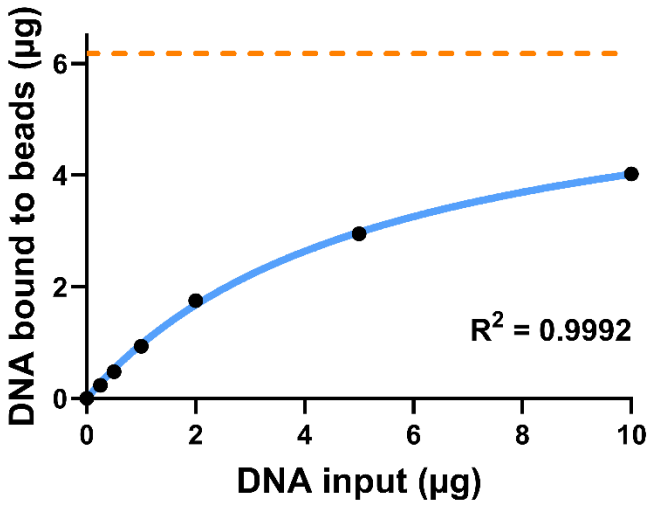

Figure 20. Test of streptavidin beads binding capacity. Different amounts of biotinylated nucleosomes were incubated with 5 µl of streptavidin beads suspension. The concentration of DNA in supernatant upon magnetic separation was measured using NanoDrop. Amounts of bound DNA were plotted against input DNA. A non-linear one-site specific model was used for fitting (blue curve) and maximum binding capacity was predicted (orange dashed line). Saturation was not reached, and only one replicate was performed due to limited amounts of material.

3.6 Nuclear Fractionation

Since the nucleosome-based pulldown assay is specifically aimed at the nuclear proteome, it was necessary to establish a way for effective cellular fractionation. Two alternative bensonase-free nuclear extraction protocols were evaluated in parallel. In both cases, nuclei were first isolated from HEK 293 cells by sequential centrifugation. In the first method, nuclear disruption was achieved through mild sonication, intended to rupture the nuclear envelope and release nuclear content. The second method employed micrococcal nuclease (MNase) digestion followed by inactivation of the enzyme via calcium chelation using EDTA. To confirm successful nuclear enrichment, the fractions were analyzed by Western blotting. Protein concentrations were first determined by Bradford assay to ensure equal loading. Cytosolic and nuclear markers were detected using antibodies against α-tubulin and histone H3, respectively. Both protocols achieved almost complete separation: histone H3 was strongly enriched in nuclear fractions, while α-tubulin was detected in cytosolic fractions (**Figure 21**), confirming effective nuclear isolation.

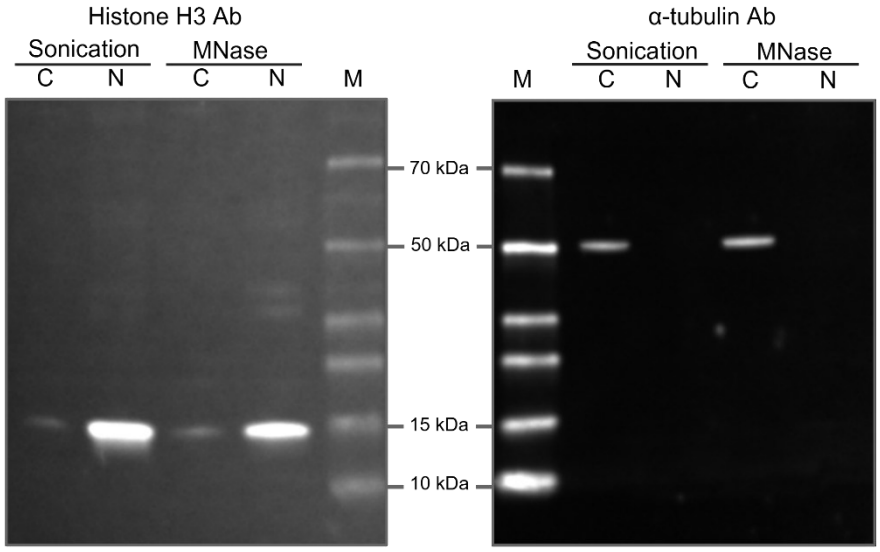

Figure 21. Western blot analysis of nuclear and cytosolic fractions obtained by two alternative benzonase-free fractionation methods. HEK 293 cells were fractionated using either sonication or micrococcal nuclease (MNase) digestion. **Left**: Detection with anti-histone H3 antibody as a nuclear marker. **Right:** Detection with anti–α-tubulin antibody as a cytosolic marker. Histone H3 was strongly enriched in nuclear fractions (N) with faint signal in cytosolic fractions (C), whereas α-tubulin was enriched in cytosolic fractions, confirming successful separation of nuclear and cytoplasmic proteins for both methods.

3.7 Dinucleosomal Arrays as a Bait for Pulldown Experiments

To evaluate whether the reconstituted, labeled dinucleosome arrays could serve as effective baits for proteomic analysis, a preliminary pulldown experiment was conducted. Biotinylated dinucleosomes with 15bp and 30bp linkers, as well as free DNA controls, were immobilized on streptavidin-coated magnetic beads and incubated with nuclear extracts from HEK 293 cells. Following incubation, beads were extensively washed to remove non-specifically bound material, and the bead-bound fractions were either submitted for mass spectrometry (results pending) or analyzed by SDS-PAGE to obtain an initial qualitative assessment of protein capture.

For each construct, samples of the post-incubation supernatant (flow-through), and triplicates of bead eluates were analyzed. SDS–PAGE revealed that, in addition to histones (strong bands at ~15 kDa), multiple other proteins were consistently captured across all three baits, with good reproducibility between technical replicates. Notably, subtle differences in profiles between the 15bp and 30 bp linker dinucleosomes were observed, suggesting linker-dependent binding (

Figure 22).

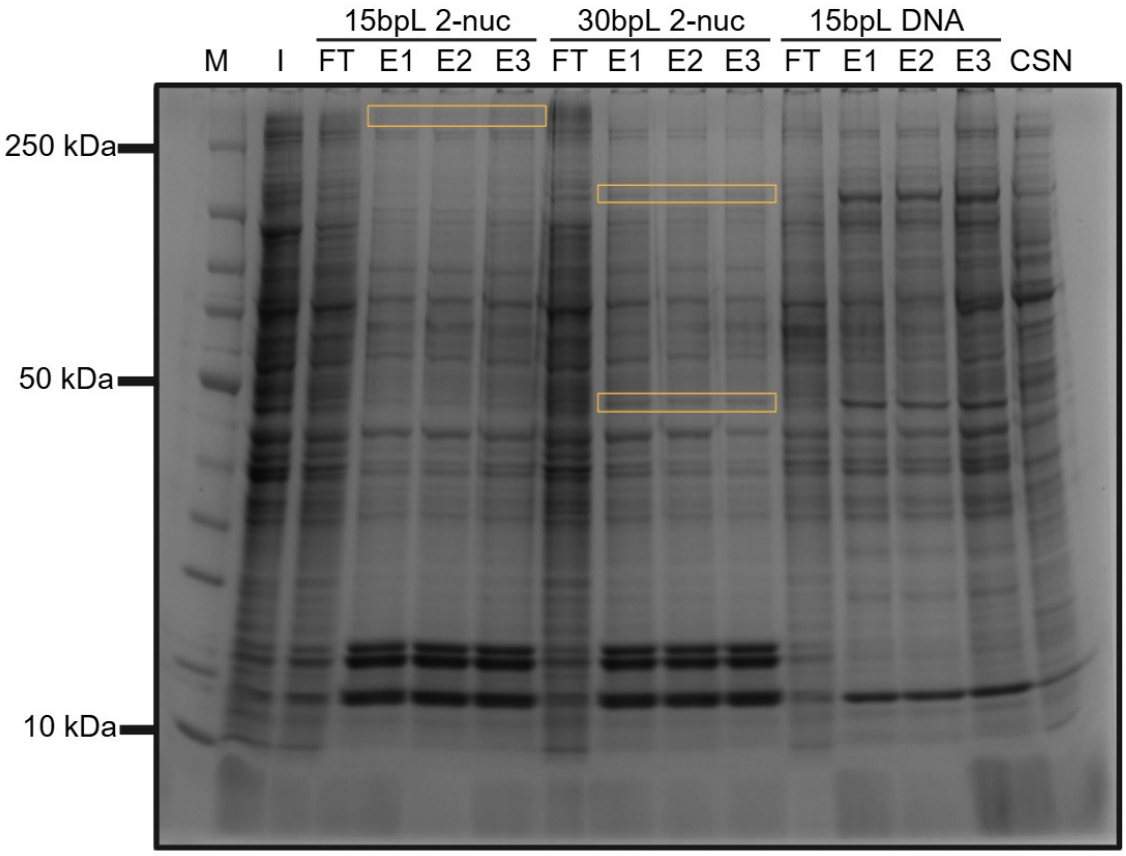

Figure 22. SDS-PAGE analysis of pilot pulldown experiment. Biotinylated nucleosomes were immobilized on streptavidin-coated magnetic beads and used as bait for affinity purification from HEK 293 nuclear extracts. The test was performed in triplicates using dinucleosomes with 15 and 30bp linkers (15bpL and 30bpL 2-nuc) along with a nucleosome-free DNA (15bpL DNA) control. After incubation with nuclear extract and magnetic separation, the supernatant was collected (FT). The different band patterns (indicated by yellow frames) in eluted material (E1, E2, E3) suggest that some nuclear proteins may exhibit linker-sensitive binding.

4 Discussion

One of the goals was to adapt a pipeline that would allow for an efficient generation of DNA constructs containing arrays with defined number of nucleosome-positioning sequences. Cloning of sequences like repetitive arrays of nucleosome-positioning Widom sequences can be challenging for several reasons, more so when aiming for full control over the length and sequence of linker DNA. According to Spakman et al. (2020) direct synthesis of repetitive sequences longer than 11 bp is challenging and not available from commercial sources. Only a single Widom sequence flanked by maximum 11bp long linkers can be directly synthesized. Direct synthesis would also be a lot more costly, and it would also lack modularity for building a library of our interest, since changing linker length or number of repeats would require full resynthesis. Linkers *in vivo* also span over a

broader range in terms of length, reaching all the way up to about 70 bp. The presented system enables precise linker expansion from a precursor construct, which contains a single Widom core sequence and the 5‘ linker. By choosing the right length of primer overhang this linker can be expanded to a defined length. PCR-based manipulation at the stage of only one Widom repeat is unproblematic, whereas at the multiplied stages that contain more than one Widom copy problems with lack of unique sequence for reannealing and primer annealing would arise. The precision of the left linker addition lies in the design of the oligo for Gibson Assembly.

For the multiplication of the Widom repeats, the use of Gibson Assembly (D. G. Gibson et al., 2009) proved to be an efficient method. Traditional ligation-based cloning could introduce unwanted restriction sites or scars when incompatible or blunt ends ligate. This would disrupt the precise control over linker length and introduce heterogeneity within linker sequences. Another problem could potentially be related to orientation control. Bi-directional cloning requires two different restriction enzyme recognition sites, hence the linkers would become heterogenous in sequence, and it could produce scars. If multiple fragments were to be ligated in a single reaction, these problems would be exacerbated by the combinatorial possibilities, and the screen for clones with the correct head-to-tail ligation would become more difficult and costly. Gibson Assembly joins DNA fragments without scaring through short homologous overlaps. This was crucial during the propagation, where the exact base-pair length of linker DNA between nucleosome-positioning sequences needed to be preserved. Maintaining defined and consistent sequences is critical to avoid introducing structural irregularities and for the downstream proteomic readout to be zoomed solely on linker DNA length. Even small variations could potentially influence spacing and orientation between neighboring nucleosomes and binding of other proteins. For this application, Gibson Assembly proved to be suitable mainly because it preserves these parameters and it makes the process fast and efficient. Importantly, pUC19 plasmid embedding allows for Sanger sequencing verification of integrity at every step using conventional M13 sequencing primers. The only step that was more difficult to execute was the first round of propagation creating a 2×Widom construct from a 1×Widom construct. For the 1×Widom construct, the insert (~230 bp) was much smaller than the plasmid backbone (~2600 bp). When the plasmid DNA was loaded for gel purification, the

insert accounted for only ~8% of the total DNA mass. This low relative abundance resulted in weak band intensity and, consequently, poor recovery during gel extraction.

For the demands of cloning and archiving, the plasmids were mostly grown and isolated at the mini-prep scale, from ~7 ml of culture. For downstream applications, specifically *in vitro* nucleosome reconstitution and pull-down experiments, the availability of milligram-scale quantities of pure plasmid DNA is required. This scale makes even the largest maxiprep commercial kits non-applicable, because of the cost and maximum yields of approximately 1 mg. The decision to perform plasmid production in liters of bacterial culture reflects these quantitative demands. The choice of traditional alkaline lysis, followed by size-selective PEG precipitation and phenol-chloroform extraction was made mainly due to its ability to perform reproducibly with high yields (~10 mg/L of culture) and high purity of recovered DNA, which is essential for preparation of DNA for enzymatic reactions and nucleosome reconstitution. The extraction ensured the correct removal of residual protein and lipid contaminants, demonstrated by the absorbance ratio values (**Table 9**). Purity of recovered DNA in terms of organic compounds used for extraction was assessed by measuring the A_{260}/A_{230} ratios, which was within acceptable limits – these contaminants could potentially inhibit sensitive downstream steps involving enzymatic reactions. The yield of the target fragment is not optimal in case of constructs containing only a single Widom copy, due to stoichiometry - most of the DNA mass comprises of the plasmid backbone, and it therefore demands high plasmid inputs to produce enough of the target construct. This could be resolved by engineering multiple copies of construct within one plasmid that can then be subsequently fragmented by restriction digestion. However, this is only suitable for generating mononucleosomal constructs, as the restriction sites for fragmentation reside within the linker DNA (as in Dyer et al., 2003). Regardless, the results validate the chosen production strategy and proved to be a reliable way for generating a set of linker-defined Widom-containing plasmids in quantities sufficient to support downstream experiments.

A crucial requirement for downstream pulldown and proteomic analysis is to efficiently isolate the Widom-containing construct from the plasmid vector and to specifically label the insert, while keeping the remaining plasmid backbone unlabeled. The biotin was picked mainly due to its high affinity towards streptavidin (K_D ~10^{-15} M) and the chemical stability of this interaction, which minimizes the risk of losing immobilized bait during wash

steps. The presence of residual plasmid backbone in the mixture could hinder nucleosome reconstitution – backbone DNA could function as a non-specific competitor for histone octamers, especially if present in larger quantities even though it is not sequence-optimized for octamer wrapping. It could reduce the effective concentration of octamers available for wrapping by the Widom DNA and lead to additional nucleosomal species. Even though these species would most probably be eliminated in the immobilization step due to absence of biotin, it would sequester histone octamers and lead to under-saturated assembly and cause the reconstitution process to be less efficient.

The initial set of tested strategies based on ligation of short DNA adapters designed against a specific overhang was intended to carry an advantageous feature. Since the 5' end of the construct contains a variable linker, the idea was to use DNA adapters of specific length to compensate for the differences in distance between bead and first nucleosome upon immobilization. However, these strategies faced inherent challenges related to ligation of cohesive ends – despite using a large molar excess of DNA adapters, religation of the backbone and formation of other unwanted byproducts dominated the reaction (**Figure 15B,C,D**).

Strategies A and B involved a double digest to cleave out a short 30bp fragment to create asymmetric cohesive ends and to favor correct ligation of adapters. This short fragment had to be separated, because it also carried the HindIII overhang, and traces of this fragment would get ligated with the adapter. Separation based on size-selective PEG precipitation and its verification appeared to be inconsistent and would require further optimization. Short adapter sequences do not contribute much to the gel shift, which complicates the readout of ligation product verification. Moreover, ligation reaction between adapter and linearized vector produced several byproducts, most notably the head-to-head dimer of target constructs. This one in would be particularly problematic in nucleosome reconstitution, as it contains twice the number of nucleosome-positioning sequences and would therefore sequester a large portion of histone octamers without carrying the biotin label for immobilization. Another complication was that this byproduct was relatively similar in size to the target construct causing problematic separation.

In Strategy B an enzymatic dephosphorylation step was added before cleaving the 26bp fragment out from the linearized plasmid to prevent recircularization or ligation of two

linearized plasmid via RS1 overhangs. Strategy C with rearranged steps presented an effort to reduce the number of non-reliable precipitation steps and to eliminate the need for 26bp fragment removal and its verification. It was also meant to place the ligation step at the very end of the pipeline to minimize loss of labeled material during anion-exchange chromatography separation and precipitation. It started with a cut at RS4 followed by dephosphorylation of DNA to prevent the already lower probability of recircularization via blunt ends. Since this procedure kept the number of DNA species lower, only needing to separate the 400bp fragment from significantly larger 2600bp backbone, the previously tested resolution of anion-exchange chromatography was sufficient. Careful monitoring of UV absorbance and salt gradient control proved essential in isolating clean, label-ready DNA (**Figure 14**). However, even with a sole isolated target fragment with one end dephosphorylated the ligation reaction produced the head-to-head byproduct. It did so even in the presence of a large molar excess of the DNA adapter. This suggests that either the ends were not sufficiently dephosphorylated, or the reaction conditions favored bimolecular ligation of vector fragments. Excessive amounts of unreacted biotinylated adapters would then most probably outcompete the target fragment during immobilization on beads. The adapter ligation-based approach was deemed inefficient. These technical limitations illustrate a bottleneck when transitioning from plasmid-embedded to free DNA for downstream biochemical use: any impurity or aberrant ligation will reduce the labeling efficiency, decrease the efficiency of nucleosome reconstitution, and impair downstream immobilization on streptavidin-coated beads. Future optimization that could help this to work would include further adjusting insert-to-vector ratios or modifying reaction conditions to suppress unwanted ligation products. Theoretically, if the phosphate group essential for ligation was not present on the cohesive end of the recipient plasmid due to dephosphorylation, but instead on the commercially synthesized DNA adapter, it could eliminate formation of the Widom-containing head-to-head byproduct. On the other hand, a new byproduct would arise in the form of the adapter ligated together, forming a species that could potentially be less problematic to separate because of its relatively small size (about 30-70 bp). Nonetheless, a large fraction of the labeled adaptor would be wasted due to self-ligation, and obtaining commercially synthesized oligonucleotides with two terminal modifications would be costly.

A commonly used procedure for terminal labeling of DNA by biotin involves PCR-based amplification via biotinylated primers. Yet it would be only applicable to this problem in the case of mononucleosomal templates. The increasing number of Widom repeats would cause a lack of unique sequences for primer annealing and could lead to amplification of constructs containing various number of Widom repeats within the mixture. The design of reverse primer would be especially difficult, because the 5‘ end of the construct contains a Gibson region, which is intentionally derived from the Widom sequence to allow repeat multiplication. This homology would cause the primer to anneal less specifically causing improper amplification. Additionally, during reannealing Widom sequences could hybridize with each other with an offset causing yet again amplification of a heterogenous mixture of N× Widom constructs, which would on a gel manifest as a ladder pattern.

A move from this multistep separation and ligation procedure was made towards a labeling strategy based on 5‘ overhang fill-in by Klenow fragment. By filling in EcoRI overhangs with biotinylated dUTP in a single enzymatic step, the need for annealing, dephosphorylation, specific cohesive ends, and ligation altogether was eliminated. This method simplifies the workflow and significantly improves the efficiency of biotin incorporation. Since Klenow-mediated labeling uses a polymerase reaction instead of a ligation equilibrium, it is driven to completion, consistent with the observed near-total DNA depletion from the supernatant after streptavidin-coated beads pulldown (**Figure 17B**). This approach exploited the previously optimized anion-exchange chromatography separation to purify the target fragment away from the large plasmid backbone. Based on its simplicity and efficiency, this enzymatic end-labeling method was selected as the preferred strategy for biotinylating DNA constructs for downstream immobilization.

Evaluation of octamer:DNA molar ratios for nucleosome reconstitutions using two different methods revealed the key characteristics of this procedure. The initial experiment using stepwise dilution at a 1:1 molar ratio showed an incomplete assembly, but it was useful to confirm the integrity and compatibility of components. The presence of free DNA and several intermediates could be caused by inefficient or hindered assembly. Gradient dialysis enabled a more controlled way for reconstitution better suited for reproducible assembly. A more systematic testing of different ratios showed that undersaturation of DNA with histone octamers leads to partial assembly – possibly populations of variously positioned mononucleosomes – and residual free DNA. On the other hand, molar excess

of octamers leads to smearing, most likely caused by non-specific aggregation of histone proteins. The optimization aimed at saturation without introducing excess histone-related aggregates and was used for subsequent large-scale reconstitution. Consistently, the same conditions yielded pure dinucleosomes when the scale was enlarged, highlighting scalability of the procedure.

An essential component of the pipeline is the immobilization of biotinylated nucleosomes on streptavidin-coated beads. The titration assay helped to estimate the approximate binding capacity of the beads for nucleosomal substrates, which is critical to avoid bead saturation or underloading in pulldown experiments. The observation that full saturation was not reached within the tested DNA input range suggests that future experiments should explore higher concentrations or alternative bead volumes to reach the binding plateau. Due to limited amounts of labeled material, it was only possible to perform this experiment without a proper number of replicates. Additionally, the current analysis focused on DNA quantification as a proxy for nucleosome binding. Incorporating histone-specific detection, for example anti-H3 Western blot of bead-bound material, would help confirm that intact nucleosomes are immobilized.

Establishing a reliable method for nuclear fractionation is crucial to ensure the relevance of nucleosome-based pulldowns, because the aim is to map interactions within the nuclear proteome. The two tested bensonase-free protocols based on sonication and MNase digestion of genomic DNA both successfully enabled nuclear protein extraction. Western blot analysis provided evidence of effective separation of nuclear and cytoplasmic contents in both approaches. While both methods performed well in terms of fractionation, they differ in their mechanisms and possibly in the yielded protein complexes. Traditional protocols often rely on bensonase digestion to degrade DNA and facilitate nuclear extraction. However, this approach is incompatible with our experiment, as our bait consists of nucleosomes, whose structural integrity is essential for studying the potential influence of linker DNA on protein binding. Bensonase non-specifically digests nucleic acids, including both free DNA and nucleosome-bound DNA. Furthermore, the enzyme itself could persist as a major protein contaminant, complicating downstream mass spectrometry by contributing to false positives. Unlike bensonase, MNase activity can be inhibited by chelation of divalent cations, and it can also be used in lower quantities, so it would present lower contamination in the analysis. Since the sonication-based protocol yielded

comparable nuclear enrichment, its use was opted for, mostly because it does not introduce additional protein into the sample.

The preliminary pulldown experiment demonstrated that linker-defined dinucleosomes can capture chromatin-associated proteins from nuclear lysates, showing that the system has potential to serve as a valid method for upcoming proteomic analysis using mass spectrometry. However, to draw conclusions about biology, the full proteomic analysis will need to be done with a sufficient number of replicates. This system has no ambition to replicate the LLPS behavior trends discussed by Gibson et al. (2019), because the nature of this experiment does not allow to have full control over salt conditions. However, the observed differences in profiles for 15bp and 30bp linker dinucleosomes may still reflect a difference in structure or accessibility that influence protein recruitment. A limitation of this system lies in the fact that at this stage only dinuclesomal arrays were tested, whereas for biochemistry and simulations in works by Gibson et al. (2019) and Chen et al. (2025) arrays of 12 nucleosomes were examined. Nevertheless, the cycling procedure that was applied for multiplication of Widom repeats with defined linkers enables assembly of any number of repeats, therefore creating a longer DNAs should not be problematic. In fact, Spakman et al. (2020) demonstrated successful assembly of 12×Widom arrays using this approach. Taken that quantization patterns of 10n+5 versus 10n impact the stacking and regular compacted fiber formation caused mainly by the varying availability of nucleosomal surfaces (Chen et al., 2025) (**Figure 4B**), arrays longer than 2 nucleosomes should be capable of capturing whether spacing-dependent binding is influenced by this feature. We hypothesize that internucleosomal spacing can influence spatial reach of proteins that contain structured modules separated by long intrinsically disordered regions. This potential sensing mechanism may not fully rely on chromatin fiber folding and could also be detectable on linear arrays. Some chromatin remodelers, such as INO80 or Chd1, contain ruler-like elements (Oberbeckmann et al., 2021). If any chromatin-associated proteins are equipped with analogous modules - a readout ruler or a flexible ruler - their binding to differently spaced nucleosomes can be highly impacted. Only quantitative proteomic analysis will determine whether linker length sensitivity in protein binding is present, and if so, whether the effect is gradual or exhibits a threshold behavior.

Alternatively, structural evidence supports the idea that linker length can directly alter binding interfaces. For example, a cryo-EM study (Dombrowski et al., 2022) of tri- and tetranucleosomal arrays with increasing linker lengths (30, 40, 50 and 60 bp) and human histone H1 revealed that the binding of H1 was impacted by linker length. In these arrays, nucleosomes 1 and 3 formed a stack, and nucleosomes 2 and 4 were extending from the stack forming a zig-zag arrangement. Nucleosome 2 was rotated relative to the stack and as linker length increases the distance from the stack increases as well. H1 binding to stacked nucleosome in these arrays (at the DNA entry site) was determined by linker DNA trajectory, which is in turn influenced by length (**Figure 23**). This raises the question of whether any chromatin-associated factors with structural homology to histone H1 or those containing a winged-helix fold also exhibit linker-sensitive binding. DNA constructs with 4×Widom repeats and variable linkers presented in this project (**Figure 8B**) set a platform to address this potential binding behavior.

A related study by Lukauskas et al. (2024) used an affinity purification approach similar to the one presented to profile combinatorial histone PTM readout on dinucleosomal arrays. The study also touched on the role of linker DNA length and found that within the range of linker lengths (35 to 55bp) the PTMs acted independently, since binding of heterochromatin or active promoter signatures was not impacted by differences in spacing. Within this range, the torsional rigidity of linker DNA is lower (Chen et al., 2025), and thus the

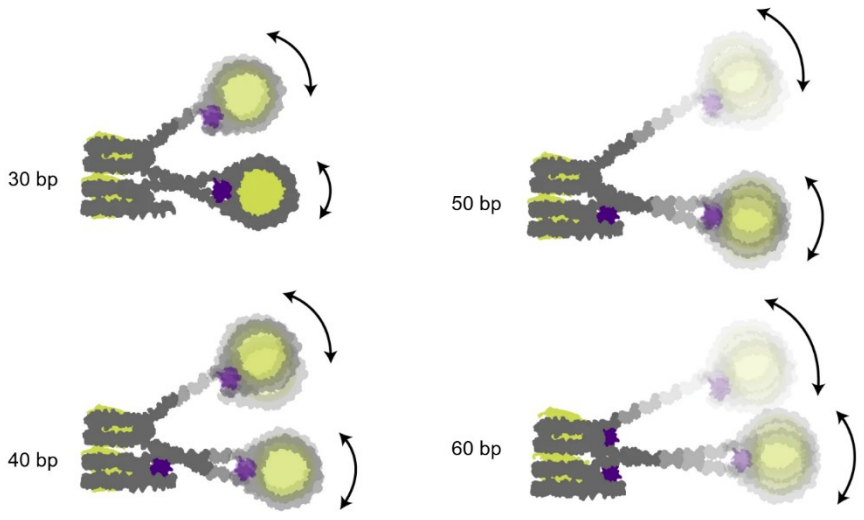

Figure 23. Histone H1 binding to tetranucleosome arrays with variable linker lengths. Binding of H1 to stacked nucleosomes 1 and 3 depends on the length of linker DNA. Longer linkers alter DNA trajectory and geometry at DNA entry sites sterically enabling contacts between H1 and DNA. Adapted from Dombrowski et al. (2022).

experiment could have missed proteins that are more sensitive to linker length changes. These potentially overlooked binders may be captured by nucleosomal arrays developed in this project with linkers spanning the range of 15 to 35 bp. Moreover, combining linker length variation within this interval with defined histone PTM patterns could uncover combinatorial effects that were overlooked. This combinatorial approach could identify protein complexes whose binding requires a particular epigenetic context and better reflects the complexity of chromatin regulation *in vivo*.

The biotinylated arrays with defined linker lengths developed during this project have potential for applications other than mass spectrometry experiments. System could also be applied to real-time kinetic measurements using biolayer interferometry and or surface plasmon resonance. Such assays would allow determination association and dissociation kinetics for linker-sensitive proteins. The arrays could also be utilized in single-molecule techniques such as optical tweezers to measuring mechanical stability in relation to linker length, or for single-molecule FRET measurements. Moreover, the system could be exploited for structural analyses by cryo-electron microscopy. Immobilization on beads can help with sample preparation and localization of target molecules (Arimura et al., 2025). Together, these potential applications illustrate that the system is not only a useful tool for proteomic profiling, but can be a versatile system that could help studying relationships between chromatin structure, dynamics, and factor recruitment at a broader level.

5 Summary

Native chromatin is a heterogeneous polymer with multiple layers of tunability, exhibiting local variations in histone composition, nucleosome positioning, DNA sequence, and post-translational modifications (PTMs). This complexity makes it challenging to decipher the physical principles of chromatin organization and the biological significance of its states in regulating DNA-associated processes. Simplified *in vitro* systems based on reconstituted nucleosome arrays provide ways to isolate individual variables and study their specific contributions. Such model systems have revealed that chromatin can undergo reversible aggregation into liquid-like condensates, with these properties being strongly influenced by the length of linker DNA. In eukaryotes, the linkers are highly variable across genomes, cell types and organisms, but globally display an oscillatory pattern with

enrichment at 10n+5 and depletion at 10n bp. Structural studies and simulations suggest that these extremes alter the rotational positioning and geometry of arrays. However, the extent to which chromatin-binding proteins can distinguish between these configurations remains unknown.

This project sought to address this gap by developing a simplified *in vitro* system of nucleosomal arrays with variable spacing, designed for use as bait in affinity purifications followed by differential proteomic analysis. The aim was to test whether linker length could serve as a discriminating factor for protein binding. To this end, a two-dimensional library of DNA constructs was assembled, based on nucleosome-positioning Widom sequences with variable linkers, using a PCR- and Gibson Assembly-based strategy for linker-length tuning and multiplication of Widom repeats to a defined number. For terminal biotinylation of DNA to enable bead immobilization, several approaches were tested. Ligation of biotinylated adapters was found to be inefficient and labor-intensive, producing unwanted by-products that could hinder downstream steps. Instead, a Klenow fragment fill-in of DNA overhangs was adopted as a more efficient alternative.

Nucleosomes with variable spacing were successfully prepared by combining biotinylated DNA constructs with refolded histone octamers. For the pulldown experiments, two benzonase-free (mass spectrometry-compatible) nuclear extraction protocols were tested and confirmed to enrich nuclear content. A preliminary feasibility pulldown experiment demonstrated promising PAGE profiles, showing that proteins were successfully captured and that certain proteins preferentially bound to nucleosomes of specific spacing. These results provide a strong foundation for the intended proteomic analysis via mass spectrometry.

6 References

Asterisk by the year of publication (Year*) marks secondary sources.

Abdulhay, N. J., Hsieh, L. J., McNally, C. P., Ostrowski, M. S., Moore, C. M., Ketavarapu, M., Kasinathan, S., Nanda, A. S., Wu, K., Chio, U. S., Zhou, Z., Goodarzi, H., Narlikar, G. J., & Ramani, V. (2023). Nucleosome density shapes kilobase-scale regulation by a mammalian chromatin remodeler. *Nature Structural & Molecular Biology*, *30*(10), 1571–1581. https://doi.org/10.1038/s41594-023-01093-6

Arimura, Y., Konishi, H. A., & Funabiki, H. (2025). MagIC-Cryo-EM: Structural determination on magnetic beads for scarce macromolecules in heterogeneous samples. *bioRxiv*, 2024.01.21.576499. https://doi.org/10.1101/2024.01.21.576499

Baldi, S., Korber, P., & Becker, P. B. (2020*) Beads on a string—Nucleosome array arrangements and folding of the chromatin fiber. *Nature Structural & Molecular Biology*, *27*(2), 109–118. https://doi.org/10.1038/s41594-019-0368-x

Baldi, S., Krebs, S., Blum, H., & Becker, P. B. (2018). Genome-wide measurement of local nucleosome array regularity and spacing by nanopore sequencing. *Nature Structural & Molecular Biology*, *25*(9), 894–901. https://doi.org/10.1038/s41594-018-0110-0

Bass, M. V., Nikitina, T., Norouzi, D., Zhurkin, V. B., & Grigoryev, S. A. (2019). Nucleosome spacing periodically modulates nucleosome chain folding and DNA topology in circular nucleosome arrays. *Journal of Biological Chemistry*, *294*(11), 4233–4246. https://doi.org/10.1074/jbc.RA118.006412

Bradford, M. M. (1976). A rapid and sensitive method for the quantitation of microgram quantities of protein utilizing the principle of protein-dye binding. *Analytical Biochemistry*, *72*, 248–254. https://doi.org/10.1016/0003-2697(76)90527-3

Brahma, S., Udugama, M. I., Kim, J., Hada, A., Bhardwaj, S. K., Hailu, S. G., Lee, T.-H., & Bartholomew, B. (2017). INO80 exchanges H2A.Z for H2A by translocating on DNA proximal to histone dimers. *Nature Communications*, *8*(1), 15616. https://doi.org/10.1038/ncomms15616

Brambilla, F., Garcia-Manteiga, J. M., Monteleone, E., Hoelzen, L., Zocchi, A., Agresti, A., & Bianchi, M. E. (2020). Nucleosomes effectively shield DNA from radiation damage in living cells. *Nucleic Acids Research*, *48*(16), 8993–9006. https://doi.org/10.1093/nar/gkaa613

Brogaard, K., Xi, L., Wang, J.-P., & Widom, J. (2012). A map of nucleosome positions in yeast at base-pair resolution. *Nature*, *486*(7404), 496–501. https://doi.org/10.1038/nature11142

Brouwer, T., Pham, C., Kaczmarczyk, A., de Voogd, W.-J., Botto, M., Vizjak, P., Mueller-Planitz, F., & van Noort, J. (2021). A critical role for linker DNA in higher-order folding of chromatin fibers. *Nucleic Acids Research*, *49*(5), 2537–2551. https://doi.org/10.1093/nar/gkab058

Chatterjee, N., Sinha, D., Lemma-Dechassa, M., Tan, S., Shogren-Knaak, M. A., & Bartholomew, B. (2011). Histone H3 tail acetylation modulates ATP-dependent remodeling through multiple mechanisms. *Nucleic Acids Research*, *39*(19), 8378–8391. https://doi.org/10.1093/nar/gkr535

Chen, L., Maristany, M. J., Farr, S. E., Luo, J., Gibson, B. A., Doolittle, L. K., Espinosa, J. R., Huertas, J., Redding, S., Collepardo-Guevara, R., & Rosen, M. K. (2025). Nucleosome spacing can fine-tune higher-order chromatin assembly. *Nature Communications*, *16*(1), 6315. https://doi.org/10.1038/s41467-025-61482-x

Chereji, R. V., Ramachandran, S., Bryson, T. D., & Henikoff, S. (2018). Precise genome-wide mapping of single nucleosomes and linkers in vivo. *Genome Biology*, *19*(1), 19. https://doi.org/10.1186/s13059-018-1398-0

Chua, E. Y. D., Vasudevan, D., Davey, G. E., Wu, B., & Davey, C. A. (2012). The mechanics behind DNA sequence-dependent properties of the nucleosome. *Nucleic Acids Research*, *40*(13), 6338–6352. https://doi.org/10.1093/nar/gks261

Clapier, C. R., Iwasa, J., Cairns, B. R., & Peterson, C. L. (2017). Mechanisms of action and regulation of ATP-dependent chromatin-remodelling complexes. *Nature Reviews Molecular Cell Biology*, *18*(7), 407–422. https://doi.org/10.1038/nrm.2017.26

Clark, S. C., Chereji, R. V., Lee, P. R., Fields, R. D., & Clark, D. J. (2020). Differential nucleosome spacing in neurons and glia. *Neuroscience Letters*, *714*, 134559. https://doi.org/10.1016/j.neulet.2019.134559

Clarkson, C. T., Deeks, E. A., Samarista, R., Mamayusupova, H., Zhurkin, V. B., & Teif, V. B. (2019). CTCF-dependent chromatin boundaries formed by asymmetric nucleosome arrays with decreased linker length. *Nucleic Acids Research*, *47*(21), 11181–11196. https://doi.org/10.1093/nar/gkz908

Correll, S. J., Schubert, M. H., & Grigoryev, S. A. (2012). Short nucleosome repeats impose rotational modulations on chromatin fibre folding. *The EMBO Journal*, *31*(10), 2416–2426. https://doi.org/10.1038/emboj.2012.80

Dombrowski, M., Engeholm, M., Dienemann, C., Dodonova, S., & Cramer, P. (2022). Histone H1 binding to nucleosome arrays depends on linker DNA length and trajectory. *Nature Structural & Molecular Biology*, *29*(5), Article 5. https://doi.org/10.1038/s41594-022-00768-w

Dyer, P. N., Edayathumangalam, R. S., White, C. L., Bao, Y., Chakravarthy, S., Muthurajan, U. M., & Luger, K. (2003). Reconstitution of Nucleosome Core Particles from Recombinant Histones and DNA. In *Methods in Enzymology* (Vol. 375, pp. 23–44). Academic Press. https://doi.org/10.1016/S0076-6879(03)75002-2

Eaton, M. L., Galani, K., Kang, S., Bell, S. P., & MacAlpine, D. M. (2010). Conserved nucleosome positioning defines replication origins. *Genes & Development*, *24*(8), 748–753. https://doi.org/10.1101/gad.1913210

Gibson, B. A., Doolittle, L. K., Schneider, M. W. G., Jensen, L. E., Gamarra, N., Henry, L., Gerlich, D. W., Redding, S., & Rosen, M. K. (2019). Organization of Chromatin by Intrinsic and Regulated Phase Separation. *Cell*, *179*(2), 470-484.e21. https://doi.org/10.1016/j.cell.2019.08.037

Gibson, D. G., Young, L., Chuang, R.-Y., Venter, J. C., Hutchison, C. A., & Smith, H. O. (2009). Enzymatic assembly of DNA molecules up to several hundred kilobases. *Nature Methods*, *6*(5), 343–345. https://doi.org/10.1038/nmeth.1318

Goldman, J. A., Garlick, J. D., & Kingston, R. E. (2010). Chromatin Remodeling by Imitation Switch (ISWI) Class ATP-dependent Remodelers Is Stimulated by Histone Variant H2A.Z. *Journal of Biological Chemistry*, *285*(7), 4645–4651. https://doi.org/10.1074/jbc.M109.072348

Hennig, B. P., Bendrin, K., Zhou, Y., & Fischer, T. (2012). Chd1 chromatin remodelers maintain nucleosome organization and repress cryptic transcription. *EMBO Reports*, *13*(11), 997–1003. https://doi.org/10.1038/embor.2012.146

Hou, Z., Nightingale, F., Zhu, Y., MacGregor-Chatwin, C., & Zhang, P. (2023). Structure of native chromatin fibres revealed by Cryo-ET in situ. *Nature Communications*, *14*(1), 6324. https://doi.org/10.1038/s41467-023-42072-1

Jambhekar, A., Dhall, A., & Shi, Y. (2019*) Roles and regulation of histone methylation in animal development. *Nature Reviews Molecular Cell Biology*, *20*(10), Article 10. https://doi.org/10.1038/s41580-019-0151-1

Klemm, S. L., Shipony, Z., & Greenleaf, W. J. (2019*). Chromatin accessibility and the regulatory epigenome. *Nature Reviews Genetics*, *20*(4), Article 4. https://doi.org/10.1038/s41576-018-0089-8

Kornberg, R. D., & Lorch, Y. (2020*) Primary Role of the Nucleosome. *Molecular Cell*, *79*(3), 371–375. https://doi.org/10.1016/j.molcel.2020.07.020

Krietenstein, N., Wal, M., Watanabe, S., Park, B., Peterson, C. L., Pugh, B. F., & Korber, P. (2016). Genomic Nucleosome Organization Reconstituted with Pure Proteins. *Cell*, *167*(3), 709-721.e12. https://doi.org/10.1016/j.cell.2016.09.045

Kubik, S., Bruzzone, M. J., Challal, D., Dreos, R., Mattarocci, S., Bucher, P., Libri, D., & Shore, D. (2019). Opposing chromatin remodelers control transcription initiation frequency and start site selection. *Nature Structural & Molecular Biology*, *26*(8), 744–754. https://doi.org/10.1038/s41594-019-0273-3

Kubik, S., O'Duibhir, E., Jonge, W. J. de, Mattarocci, S., Albert, B., Falcone, J.-L., Bruzzone, M. J., Holstege, F. C. P., & Shore, D. (2018). Sequence-Directed Action of RSC Remodeler and General Regulatory Factors Modulates +1 Nucleosome Position to Facilitate Transcription. *Molecular Cell*, *71*(1), 89-102.e5. https://doi.org/10.1016/j.molcel.2018.05.030

Lai, B., Gao, W., Cui, K., Xie, W., Tang, Q., Jin, W., Hu, G., Ni, B., & Zhao, K. (2018). Principles of nucleosome organization revealed by single-cell micrococcal nuclease sequencing. *Nature*, *562*(7726), 281–285. https://doi.org/10.1038/s41586-018-0567-3

Lantermann, A. B., Straub, T., Strålfors, A., Yuan, G.-C., Ekwall, K., & Korber, P. (2010). Schizosaccharomyces pombe genome-wide nucleosome mapping reveals positioning mechanisms distinct from those of Saccharomyces cerevisiae. *Nature Structural & Molecular Biology*, *17*(2), 251–257. https://doi.org/10.1038/nsmb.1741

Levendosky, R. F., Sabantsev, A., Deindl, S., & Bowman, G. D. (2016). The Chd1 chromatin remodeler shifts hexasomes unidirectionally. *eLife*, *5*, e21356. https://doi.org/10.7554/eLife.21356

Lorch, Y., Maier-Davis, B., & Kornberg, R. D. (2014). Role of DNA sequence in chromatin remodeling and the formation of nucleosome-free regions. *Genes & Development*, *28*(22), 2492–2497. https://doi.org/10.1101/gad.250704.114

Lowary, P. T., & Widom, J. (1998). New DNA sequence rules for high affinity binding to histone octamer and sequence-directed nucleosome Richmond. *Journal of Molecular Biology*, *276*(1), 19–42. https://doi.org/10.1006/jmbi.1997.1494

Lukauskas, S., Tvardovskiy, A., Nguyen, N. V., Stadler, M., Faull, P., Ravnsborg, T., Özdemir Aygenli, B., Dornauer, S., Flynn, H., Lindeboom, R. G. H., Barth, T. K., Brockers, K., Hauck, S. M., Vermeulen, M., Snijders, A. P., Müller, C. L., DiMaggio, P. A., Jensen, O. N., Schneider, R., & Bartke, T. (2024). Decoding chromatin states by proteomic profiling of nucleosome readers. *Nature*, 1–9. https://doi.org/10.1038/s41586-024-07141-5

Mavrich, T. N., Ioshikhes, I. P., Venters, B. J., Jiang, C., Tomsho, L. P., Qi, J., Schuster, S. C., Albert, I., & Pugh, B. F. (2008). A barrier nucleosome model for statistical positioning of nucleosomes

throughout the yeast genome. *Genome Research*, *18*(7), 1073–1083. https://doi.org/10.1101/gr.078261.108

Misteli, T. (2007*) Beyond the Sequence: Cellular Organization of Genome Function. *Cell*, *128*(4), 787–800. https://doi.org/10.1016/j.cell.2007.01.028

Nacev, B. A., Feng, L., Bagert, J. D., Lemiesz, A. E., Gao, J., Soshnev, A. A., Kundra, R., Schultz, N., Muir, T. W., & Allis, C. D. (2019). The expanding landscape of “oncohistone” mutations in human cancers. *Nature*, *567*(7749), 473–478. https://doi.org/10.1038/s41586-019-1038-1

Nagai, S., Davis, R. E., Mattei, P. J., Eagen, K. P., & Kornberg, R. D. (2017). Chromatin potentiates transcription. *Proceedings of the National Academy of Sciences*, *114*(7), 1536–1541. https://doi.org/10.1073/pnas.1620312114

Neri, F., Rapelli, S., Krepelova, A., Incarnato, D., Parlato, C., Basile, G., Maldotti, M., Anselmi, F., & Oliviero, S. (2017). Intragenic DNA methylation prevents spurious transcription initiation. *Nature*, *543*(7643), Article 7643. https://doi.org/10.1038/nature21373

Ng, H. H., Feng, Q., Wang, H., Erdjument-Bromage, H., Tempst, P., Zhang, Y., & Struhl, K. (2002). Lysine methylation within the globular domain of histone H3 by Dot1 is important for telomeric silencing and Sir protein association. *Genes & Development*, *16*(12), 1518–1527. https://doi.org/10.1101/gad.1001502

Nizovtseva, E. V., Clauvelin, N., Todolli, S., Polikanov, Y. S., Kulaeva, O. I., Wengrzynek, S., Olson, W. K., & Studitsky, V. M. (2017). Nucleosome-free DNA regions differentially affect distant communication in chromatin. *Nucleic Acids Research*, *45*(6), 3059–3067. https://doi.org/10.1093/nar/gkw1240

Oberbeckmann, E., Niebauer, V., Watanabe, S., Farnung, L., Moldt, M., Schmid, A., Cramer, P., Peterson, C. L., Eustermann, S., Hopfner, K.-P., & Korber, P. (2021). Ruler elements in chromatin remodelers set nucleosome array spacing and phasing. *Nature Communications*, *12*(1), 3232. https://doi.org/10.1038/s41467-021-23015-0

Öberg, C., Izzo, A., Schneider, R., Wrange, Ö., & Belikov, S. (2012). Linker Histone Subtypes Differ in Their Effect on Nucleosomal Spacing *In Vivo*. *Journal of Molecular Biology*, *419*(3), 183–197. https://doi.org/10.1016/j.jmb.2012.03.007

Ocampo, J., Chereji, R. V., Eriksson, P. R., & Clark, D. J. (2016). The ISW1 and CHD1 ATP-dependent chromatin remodelers compete to set nucleosome spacing in vivo. *Nucleic Acids Research*, *44*(10), 4625–4635. https://doi.org/10.1093/nar/gkw068

Ocampo, J., Chereji, R. V., Eriksson, P. R., & Clark, D. J. (2019). Contrasting roles of the RSC and ISW1/CHD1 chromatin remodelers in RNA polymerase II elongation and termination. *Genome Research*, *29*(3), 407–417. https://doi.org/10.1101/gr.242032.118

Perišić, O., Collepardo-Guevara, R., & Schlick, T. (2010). Modeling studies of chromatin fiber structure as a function of DNA linker length. *Journal of Molecular Biology*, *403*(5), 777–802. https://doi.org/10.1016/j.jmb.2010.07.057

Piroeva, K. V., McDonald, C., Xanthopoulos, C., Fox, C., Clarkson, C. T., Mallm, J.-P., Vainshtein, Y., Ruje, L., Klett, L. C., Stilgenbauer, S., Mertens, D., Kostareli, E., Rippe, K., & Teif, V. B. (2023).

Nucleosome repositioning in chronic lymphocytic leukemia. *Genome Research*, *33*(10), 1649–1661. https://doi.org/10.1101/gr.277298.122

Pointner, J., Persson, J., Prasad, P., Norman-Axelsson, U., Strålfors, A., Khorosjutina, O., Krietenstein, N., Svensson, J. P., Ekwall, K., & Korber, P. (2012). CHD1 remodelers regulate nucleosome spacing in vitro and align nucleosomal arrays over gene coding regions in S. pombe. *The EMBO Journal*, *31*(23), 4388–4403. https://doi.org/10.1038/emboj.2012.289

Robinson, P. J. J., Fairall, L., Huynh, V. A. T., & Rhodes, D. (2006). EM measurements define the dimensions of the “30-nm” chromatin fiber: Evidence for a compact, interdigitated structure. *Proceedings of the National Academy of Sciences*, *103*(17), 6506–6511. https://doi.org/10.1073/pnas.0601212103

Satchwell, S. C., Drew, H. R., & Travers, A. A. (1986). Sequence periodicities in chicken nucleosome core DNA. *Journal of Molecular Biology*, *191*(4), 659–675. https://doi.org/10.1016/0022-2836(86)90452-3

Schones, D. E., Cui, K., Cuddapah, S., Roh, T.-Y., Barski, A., Wang, Z., Wei, G., & Zhao, K. (2008). Dynamic Regulation of Nucleosome Positioning in the Human Genome. *Cell*, *132*(5), 887–898. https://doi.org/10.1016/j.cell.2008.02.022

Sims, R. J., Chen, C.-F., Santos-Rosa, H., Kouzarides, T., Patel, S. S., & Reinberg, D. (2005). Human but not yeast CHD1 binds directly and selectively to histone H3 methylated at lysine 4 via its tandem chromodomains. *The Journal of Biological Chemistry*, *280*(51), 41789–41792. https://doi.org/10.1074/jbc.C500395200

Singh, A. K., & Mueller-Planitz, F. (2021*) Nucleosome Positioning and Spacing: From Mechanism to Function. *Journal of Molecular Biology*, *433*(6), 166847. https://doi.org/10.1016/j.jmb.2021.166847

Singh, A. K., Schauer, T., Pfaller, L., Straub, T., & Mueller-Planitz, F. (2021). The biogenesis and function of nucleosome arrays. *Nature Communications*, *12*(1), 7011. https://doi.org/10.1038/s41467-021-27285-6

Smolle, M., Venkatesh, S., Gogol, M. M., Li, H., Zhang, Y., Florens, L., Washburn, M. P., & Workman, J. L. (2012). Chromatin remodelers Isw1 and Chd1 maintain chromatin structure during transcription by preventing histone exchange. *Nature Structural & Molecular Biology*, *19*(9), 884–892. https://doi.org/10.1038/nsmb.2312

Spakman, D., King, G. A., Peterman, E. J. G., & Wuite, G. J. L. (2020). Constructing arrays of nucleosome positioning sequences using Gibson Assembly for single-molecule studies. *Scientific Reports*, *10*(1), Article 1. https://doi.org/10.1038/s41598-020-66259-4

Stockdale, C., Flaus, A., Ferreira, H., & Owen-Hughes, T. (2006). Analysis of Nucleosome Repositioning by Yeast ISWI and Chd1 Chromatin Remodeling Complexes*. *Journal of Biological Chemistry*, *281*(24), 16279–16288. https://doi.org/10.1074/jbc.M600682200

Tolstorukov, M. Y., Goldman, J. A., Gilbert, C., Ogryzko, V., Kingston, R. E., & Park, P. J. (2012). Histone Variant H2A.Bbd Is Associated with Active Transcription and mRNA Processing in Human Cells. *Molecular Cell*, *47*(4), 596–607. https://doi.org/10.1016/j.molcel.2012.06.011

Torigoe, S. E., Patel, A., Khuong, M. T., Bowman, G. D., & Kadonaga, J. T. (2013). ATP-dependent chromatin assembly is functionally distinct from chromatin remodeling. *eLife*, *2*, e00863. https://doi.org/10.7554/eLife.00863

Tsukiyama, T., Palmer, J., Landel, C. C., Shiloach, J., & Wu, C. (1999). Characterization of the Imitation Switch subfamily of ATP-dependent chromatin-remodeling factors in Saccharomyces cerevisiae. *Genes & Development*, *13*(6), 686–697.

Udugama, M., Sabri ,Abdellah, & and Bartholomew, B. (2011). The INO80 ATP-Dependent Chromatin Remodeling Complex Is a Nucleosome Spacing Factor. *Molecular and Cellular Biology*, *31*(4), 662–673. https://doi.org/10.1128/MCB.01035-10

Valouev, A., Johnson, S. M., Boyd, S. D., Smith, C. L., Fire, A. Z., & Sidow, A. (2011). Determinants of nucleosome organization in primary human cells. *Nature*, *474*(7352), 516–520. https://doi.org/10.1038/nature10002

Vasseur, P., Tonazzini, S., Ziane, R., Camasses, A., Rando, O. J., & Radman-Livaja, M. (2016). Dynamics of Nucleosome Positioning Maturation following Genomic Replication. *Cell Reports*, *16*(10), 2651–2665. https://doi.org/10.1016/j.celrep.2016.07.083

Voong, L. N., Xi, L., Sebeson, A. C., Xiong, B., Wang, J.-P., & Wang, X. (2016a). Insights into Nucleosome Organization in Mouse Embryonic Stem Cells through Chemical Mapping. *Cell*, *167*(6), 1555-1570.e15. https://doi.org/10.1016/j.cell.2016.10.049

Voong, L. N., Xi, L., Sebeson, A. C., Xiong, B., Wang, J.-P., & Wang, X. (2016b). Insights into Nucleosome Organization in Mouse Embryonic Stem Cells through Chemical Mapping. *Cell*, *167*(6), 1555-1570.e15. https://doi.org/10.1016/j.cell.2016.10.049

Weiner, A., Hughes, A., Yassour, M., Rando, O. J., & Friedman, N. (2010). High-resolution nucleosome mapping reveals transcription-dependent promoter packaging. *Genome Research*, *20*(1), 90–100. https://doi.org/10.1101/gr.098509.109

Yang, J. G., Madrid, T. S., Sevastopoulos, E., & Narlikar, G. J. (2006). The chromatin-remodeling enzyme ACF is an ATP-dependent DNA length sensor that regulates nucleosome spacing. *Nature Structural & Molecular Biology*, *13*(12), 1078–1083. https://doi.org/10.1038/nsmb1170

Yuan, G.-C., Liu, Y.-J., Dion, M. F., Slack, M. D., Wu, L. F., Altschuler, S. J., & Rando, O. J. (2005). Genome-Scale Identification of Nucleosome Positions in S. cerevisiae. *Science*, *309*(5734), 626–630. https://doi.org/10.1126/science.1112178